Available online at www.sciencedirect.com

ScienceDirect

Geochimica et Cosmochimica Acta 325 (2022) 106–128

Geochimica et Cosmochimica Acta

www.elsevier.com/locate/gca

Characterization of achondritic cosmic spherules from the Widerøefjellet micrometeorite collection (Sør Rondane Mountains, East Antarctica)

Bastien Soens [a,b,*], Stepan M. Chernonozhkin [c,d], Claudia González de Vega [c], Frank Vanhaecke [c], Matthias van Ginneken [e], Philippe Claeys [a], Steven Goderis [a]

[a] *Analytical-, Environmental-, and Geo-Chemistry, Vrije Universiteit Brussel, Pleinlaan 2, BE-1050 Brussels, Belgium*
[b] *Laboratoire G-Time, Université Libre de Bruxelles 50, Av. F.D. Roosevelt CP 160/02, BE-1050 Brussels, Belgium*
[c] *Department of Chemistry, Ghent University, Krijgslaan 218 Building S12, BE-9000 Gent, Belgium*
[d] *Chair of General and Analytical Chemistry, Research Group - Isotope Ratio Analysis, Montanuniversität Leoben, Franz Josef-Straße 18, 8700 Leoben, Austria*[1]
[e] *Centre for Astrophysics and Planetary Science, University of Kent, CT2 7NZ Canterbury, Kent, United Kingdom*

Received 5 August 2021; accepted in revised form 23 March 2022; available online 29 March 2022

Abstract

Achondritic micrometeorites represent one of the rarest (ca. 0.5–2.1%) particle types among Antarctic micrometeorite collections. Here, we present major, trace element and oxygen isotope compositions on five vitreous, achondritic cosmic spherules (341–526 μm in size) recovered from the Widerøefjellet sedimentary trap in the Sør Rondane Mountains (SRMs) of East Antarctica. We also present the first iron isotope data for four of these achondritic cosmic spherules. The particles were initially identified based on the atomic concentrations of Fe-Mg-Mn and their distribution in Fe/Mg versus Fe/Mn space, spanning a relatively wide range in Fe/Mg ratios (ca. 0.48–1.72). The Fe/Mn ratios cover a more restricted range (22.4–31.7), comparable to or slightly below the values measured for howardite-eucrite-diogenite (HED) and martian meteorites. One particle (WF1801-AC3) displays an elevated Fe/Mn ratio of ~78, comparable to the values determined for lunar rocks. The negative correlation observed between the $CaO + Al_2O_3$ contents and the Fe/Si ratios of achondritic spherules reflects both the mineralogy of the precursor materials, as well as the extent of volatilization experienced during atmospheric entry heating. This trend suggests that the primary mineralogy of precursor materials may have been compositionally similar to basaltic achondrites. Based on their distribution in Ca/Si versus Al/Si space, we argue that the majority of achondritic cosmic spherules predominantly sample pyroxene- and/or plagioclase-rich (i.e., basaltic) precursor bodies. Such precursor mineralogy is also inferred from their rare earth element (REE) patterns, which show resemblances to fine-grained basaltic eucrites or Type 1 achondritic spherules ($n = 3$ – av. $REE_N = 11.2$–15.5, $(La/Yb)_N = 0.93$–1.21), pigeonite-rich equilibrated eucrite precursors or Type 2 achondritic spherules ($n = 1$ – av. $REE_N = 27.9$, $(La/Yb)_N = 0.10$), and possibly Ca-phosphates from (primitive) achondritic bodies (n = 1 – av. $REE_N = 58.8$, $(La/Yb)_N = 1.59$). This is clearly demonstrated for particle WF1801AC-1, which was likely inherited from a fine-grained eucritic precursor body. The pre-atmospheric oxygen isotope composition was reconstructed through compensation of mass-dependent fractionation processes as well as mixing with atmospheric oxygen, using iron isotope data. Two particles (WF1801AC-2, WF1801-AC4) display corrected oxygen isotope compositions ($\delta^{18}O = 3.7$–4.4‰) largely consistent with HED meteorites and may thus originate from HED-like parent bodies. The corrected oxygen isotope compositions ($\delta^{18}O = 12.6$–12.8‰) of the remaining particles (WF1801-AC3, WF1801-AC5) do not

* Corresponding author at: Analytical-, Environmental-, and Geo-Chemistry, Vrije Universiteit Brussel, Pleinlaan 2, BE-1050 Brussels, Belgium.

E-mail address: Bastien.Soens@vub.be (B. Soens).

[1] Current address.

https://doi.org/10.1016/j.gca.2022.03.029
0016-7037/© 2022 Elsevier Ltd. All rights reserved.

correspond to known meteorite fields and may represent two distinct types of unknown achondritic parent bodies or residual atmospheric entry effects. Finally, the abundance (ca. 0.5%) of achondritic cosmic spherules within the Widerøefjellet sedimentary trap is comparable to that observed in the South Pole Water Well (SPWW – ca. 0.5%), Novaya Zemlya glacier (ca. 0.45%) and Transantarctic Mountain (TAM) (ca. 2.1%) collections, confirming their overall rarity in micrometeorite collections. Unambiguous evidence for micrometeorites from the Moon or Mars remains absent from collections to date.
© 2022 Elsevier Ltd. All rights reserved.

Keywords: Oxygen isotopes; Iron isotopes; Achondrites; Cosmic spherules; Atmospheric entry

1. INTRODUCTION

Achondrite (or differentiated meteorites) is a collective term for meteoritic fragments characterized by igneous textures, which have sampled (partially) differentiated asteroids or planetary bodies (Mittlefehldt et al., 1998; Weisberg et al., 2006). They generally lack mm-sized, igneous droplets or 'chondrules', which are commonly observed within the majority of chondritic meteorites, and display more evolved, non-solar-like compositions. This is attributed to a variety of planetary-scale differentiation processes, including core-mantle segregation and the development of a crust- and mantle-like structure through fractional melting and crystallization processes (Mittlefehldt et al., 1998), essentially destroying primary textural features and modifying the chemical and isotopic composition of the parent body material. As the formation of achondritic meteoritic materials is complex and the resulting planetary products diverse, we refer the reader to more exhaustive overviews of magma formation on planetary bodies and the range of achondrite parent bodies that have been sampled by meteorites to date (e.g., Mittlefehldt et al., 1998; Greenwood et al., 2017; Christiansen et al., 2022).

Stony achondrites sample (partial) melts, melt residues and cumulate rocks within the crust or mantle of a differentiated asteroid or planetary body. Chemically, these materials can be distinguished from their chondritic or primitive achondritic analogues based on their distribution in Fe/Mg versus Fe/Mn space (Goodrich and Delaney, 2000). The latter work has demonstrated that achondrites display a characteristic fractionation trend in their Fe/Mg composition due to different compatibilities of Fe, Mg and Mn in common mineral phases during partial melting and fractional crystallization stages. Igneous fractionation produces large variations in Fe/Mg ratios with typically more limited changes in Fe/Mn ratios, due to the generally similar crystal-chemical behaviour of Fe^{2+} and Mn^{2+} (Duke, 1976; Stolper, 1977). Variations in Fe/Mn are commonly regarded to be a consequence of volatility-controlled fractionation of Mn or to reflect primary differences in oxidation state and/or total Fe content among the materials that accreted to different parent bodies (Goodrich and Delaney, 2000). This chemical partitioning is particularly useful to determine whether differentiated meteorites sampled a crustal/evolved- (high Fe/Mg) or primitive/mantle-like (low Fe/Mg) source lithology. Furthermore, the Fe/Mn ratio is relatively constrained to specific achondritic parent bodies, which demonstrates its potential as an identification parameter (Taylor et al., 2007; Cordier et al. 2012). For instance, the howardite-, eucrite- and diogenite-suite (or HED-suite), presumed to have originated from the 4-Vesta asteroid, is characterized by relatively constant Fe/Mn ratios of 30 ± 2 (Papike et al., 2003). Similar to the HED-suite, martian or shergottite-nakhlite-chassignite (SNC) meteorites display Fe/Mn ratios of 32 ± 6. This value is considerably higher in lunar meteorites (62 ± 18) and angrites (111 ± 23; Papike et al., 2003). Here, it is important to note that exceptions to these ranges exist. First, meteorites with comparable mineralogy and Fe/Mn ratios but distinct oxygen isotope compositions relative to the HED-group have been identified (e.g., Scott et al., 2009). Such anomalous eucrites may indicate that 4-Vesta remained isotopically heterogeneous due to incomplete melting (Wiechert et al., 2004), or may alternatively suggest the existence of several asteroids with mineralogical compositions similar to that of 4-Vesta but distinct oxygen isotope compositions and differentiation histories (Scott et al., 2009; Hublet et al., 2017). Second, olivine-rich achondrites have been associated with the HED-group based on oxygen and chromium isotope systematics, extending the inventory of materials and mineralogies linked to this group (Vaci et al., 2021). Despite these limitations, the combined use of element and oxygen isotope data are considered suitable parameters for the identification of the parent body of the differentiated micrometeoroids, provided that the mineralogical control is understood (Cordier et al., 2012).

Micrometeorites are extraterrestrial dust particles 10–2000 μm in size (Rubin and Grossman, 2010), which are commonly classified into unmelted, scoriaceous and molten subtypes based on their textural properties (Kurat et al., 1994; Engrand and Maurette, 1998; Genge et al., 2008). Molten micrometeorites (commonly referred to as 'cosmic spherules') have suffered near-complete melting during atmospheric entry and have subsequently experienced (severe) textural, chemical and isotopic modifications (e.g., Folco and Cordier, 2015). Achondritic particles have previously been recovered and identified from the Antarctic micrometeorite record. Taylor et al. (2007) initially reported a small number ($n = 7$) of vitreous cosmic spherules from the highly pristine SPWW collection and observed Fe/Mn ratios comparable to HED meteorites. They argued that Mg (50% condensation temperature T_C = 1336–1343 K – Lodders, 2003; Wood et al., 2019) and Mn (50 %T_C = 1123–1158 K – Lodders, 2003; Wood et al., 2019) largely remained unaffected by atmospheric entry heating based on isotopic fractionation trends in cosmic spherules (Alexander et al., 2002; Engrand et al., 2005;

Taylor et al., 2005). However, Fe (50 %T_C = 1336–1338 K – Lodders, 2003; Wood et al., 2019) appears to be more susceptible to loss during atmospheric heating processes, including by evaporation (Engrand et al., 2005; Taylor et al., 2005) and metal bead extraction (Bi et al., 1993; Genge and Grady, 1998). Metal bead extraction may occur when micrometeoroids, enriched in fine-grained carbonaceous matter, are heated during atmospheric entry (Brownlee et al., 1997; Genge and Grady, 1998). A strongly reduced environment is formed through pyrolysis of carbonaceous material, concentrating key transitional elements (e.g., Fe, Co, Ni, V) into immiscible sulfide liquids segregated from the silicate melt due to their siderophile behaviour. Subsequently, most of the volatile sulfur evaporates and metal beads enriched in these elements are left behind and/or lost from the particle (e.g., Taylor et al, 2011; Suttle et al., 2021a,b). The aforementioned processes tend to shift the Fe/Mg and Fe/Mn ratios to lower values, but their significance is considered to be relatively minor (Taylor et al., 2007). As such, the Fe/Mg versus Fe/Mn relationships of achondritic micrometeorites are interpreted to reflect the bulk composition of the parent body.

A limited number of unmelted achondritic micrometeorites have also been recovered from the Antarctic blue ice fields at Cap Prud'homme (n = 1 – Gounelle et al., 2009) and the Russian Novaya Zemlya glacier (n = 4 – Badjukov et al., 2010). These basaltic micrometeorites have been linked to HEDs, mesosiderites or even unknown types of achondritic parent bodies, demonstrating the importance of micrometeorites in expanding the current inventory of solar system materials. More recently, Cordier et al. (2011a, 2012) have investigated the major, trace element and oxygen isotope composition of vitreous achondritic cosmic spherules from the SPWW (n = 4, 3 of which were previously studied by Taylor et al., 2007) and sedimentary traps in the TAMs (n = 12). They argued that most achondritic micrometeorites display vitreous textures due to their lower Mg contents, which lowers their melting temperature. Based on their observations, Cordier et al. (2011a, 2012) have suggested several additional parameters that may assist in the identification of achondritic micrometeorites. For instance, achondritic cosmic spherules tend to be depleted in siderophile elements (e.g., Ni: 0.17–131 μg/g and Co: 1.3–68.1 μg/g) and are enriched in the REEs (1.4–13.7x CI), which is consistent with the generation and extraction of basaltic melts from a differentiated body. Furthermore, Cordier et al. (2012) were able to distinguish three different types of precursor material based on the REE pattern of the achondritic cosmic spherules, including fine-grained eucrites consisting of pigeonite and anorthite (Type 1), pigeonite-rich eucrites (Type 2) and a howardite-like precursor containing metal-bearing diogenite fragments (Type 3). However, the oxygen isotope data measured for these achondritic cosmic spherules did not prove to be consistent with reference values for HED meteorites. This was attributed to atmospheric entry heating, which induces mass-dependent fractionation and mixing with atmospheric oxygen, consequently modifying the original oxygen isotopic composition of the precursor body (Yada et al., 2005; Suavet et al., 2010; van Ginneken et al., 2017; Goderis et al., 2020; Rudraswami et al., 2020; Suttle et al., 2020; Soens et al., 2020). Additionally, Antarctic micrometeorites may experience aqueous alteration processes, which shift the oxygen isotope composition towards alteration products in equilibrium with Antarctic meteoric water and ice (Zekollari et al., 2019; Goderis et al., 2020; Suttle et al., 2021a,b). Quantification of oxygen isotope fractionation processes is thus essential to identify the precursor body of melted (achondritic) micrometeorites. Recently, Brase et al. (2021) recovered two achondritic cosmic spherules from sedimentary deposits at Mount Raymond and the Jacobs Nunatak in the Transantarctic Mountains. They concluded that the differentiated particles presumably originated from 4-Vesta based on their major and trace element compositions.

Here, we present new major, trace element and oxygen isotope data for five vitreous achondritic cosmic spherules recovered from the Widerøefjellet sedimentary trap in the Sør Rondane Mountains of Dronning Maud Land, East Antarctica. In addition, we provide the first iron isotope data for four of these achondritic cosmic spherules. This information is useful to estimate the extent of mass-dependent fractionation processes and thus to allow a reconstruction of the pre-atmospheric oxygen isotope composition of achondritic micrometeorites. Finally, we compare the abundance of achondritic micrometeorites among the respective collection sites to investigate potential preservation or sampling biases.

2. MATERIALS AND METHODS

Extraterrestrial- and impact-related material was recently discovered in natural sedimentary traps at Widerøefjellet in the Sør Rondane Mountains (Dronning Maud Land, East Antarctica) during the MICROMETA (2012–2013) and Belgian Antarctic Meteorites and Micrometeorites (BAMM!–2018) expeditions (Goderis et al., 2020; Soens et al., 2021, van Ginneken et al., 2021). These sediment traps primarily consisted of weathering pits, exposed cracks, fissured surfaces within meta-tonalitic host rocks and moraine deposits (Kamei et al., 2013; Kojima and Shiraishi, 1986). The accumulation of microscopic dust particles in the SRMs presumably initiated ca. 1–3 Ma based on the glacial history and ^{10}Be bedrock exposure ages acquired in the western parts of the SRM (Suganuma et al., 2014). According to Goderis et al. (2020), accumulation of extraterrestrial material at this site is predominantly controlled by atmospheric infall. This was deduced from the physicochemical and isotopic properties of the Widerøefjellet cosmic spherule collection. Due to the unique environmental conditions, including the cold and dry Antarctic climate, lack of anthropogenic influence and the ability to accumulate material over a prolonged timespan, extraterrestrial material can easily be identified using a binocular microscope (e.g., based on shape, texture, etc.) and is generally omitted from significant terrestrial alteration processes. The Widerøefjellet cosmic spherule collection is thus likely to represent the modern cosmic dust flux to Earth (Taylor et al. 2000; 2007; Duprat et al., 2010; Suavet et al. 2011; Goderis et al., 2020; Rojas et al., 2021).

The bulk sedimentary deposit (ca. 2.65 kg) collected from the Widerøefjellet 1 (2018) sedimentary trap was initially weighed, washed to remove excess silt and clay particles, and sieved into six size fractions ranging from <125 μm to >2000 μm. The respective size fractions were dried in an oven at a temperature of ca. 60 °C for a time span of 12–24 hours. A magnetic separation was performed using a hand magnet to extract most magnetite-bearing micrometeorites. Magnetite is commonly formed when both ferrous and ferric iron are oxidized during atmospheric entry heating, while metallic iron is oxidized and incorporated into the silicate melt (Genge and Grady, 1999). Vitreous cosmic spherules, which do not display crystal development due to the lack of crystal nuclei and a high cooling rate, mainly reside within the non-magnetic sediment fraction. Micrometeorites from the magnetic and non-magnetic size fractions were subsequently extracted using a binocular microscope and Ti-coated tweezers to prevent contamination with siderophile elements (e.g., Ni). During this study, we have focused on vitreous cosmic spherules recovered from the non-magnetic sediment fractions based on previous observations which demonstrated that achondritic micrometeorites are predominantly vitreous (e.g., Taylor et al., 2007; Cordier et al., 2011a; 2012). This observation is supported by numerical models, although such simulations indicate that there is a significant difference between the behavior of diogenite and eucrite particles, with eucrite particles more likely to melt to form cosmic spherules than diogenite or ordinary chondrite materials (Genge, 2017). Semi-quantitative compositions were determined with a JEOL JSM IT-300 scanning electron microscope (SEM) coupled to an Oxford energy-dispersive spectrometer (EDS) at the SURF research unit of the Vrije Universiteit Brussel (VUB), Belgium. Achondritic micrometeorites were searched for using the aforementioned Fe/Mg versus Fe/Mn systematics (Goodrich and Delaney, 2000; Taylor et al., 2007). A total of five vitreous or V-type cosmic spherules (among 1000 s of chondritic particles) were identified, which display non-chondritic Fe/Mg–Fe/Mn ratios and used for further study. Table 1 provides an overview of the physical properties of these five cosmic spherules selected during this study. The particles were subsequently embedded in epoxy resin and polished for further analysis (Fig. S1).

Major and trace element compositions were analyzed *in situ* (i.e., on unaltered surfaces predominantly near the center of the particle) using a Teledyne Cetac Technologies Analyte G2 excimer-based laser ablation system equipped with HelexII double volume cell and ARIS aerosol introduction system and coupled to a Thermo Scientific Element XR sector field inductively coupled plasma–mass spectrometer (LA-ICP-MS) at the Department of Chemistry of Ghent University (Ghent, Belgium) using an external calibration curve composed of USGS (i.e., BHVO-2G, BIR-1G, GSD-1G, GSE-1G) and MPI-DING (i.e., ATHO-G, GOR132-G, ML3B-G, StHs6/80-G, T1-G) glass reference materials and established sum normalization data processing approach (Chernonozhkin et al., 2021; see Table S1). To remove potential adhesives on the surface of micrometeorites, a short pre-ablation procedure was run prior to LA-ICP-MS analysis. Three replicate analyses were performed using a spot size of ca. 35 μm. Values reported in Table S1 represent average values for the respective particles. The accuracy of the LA-ICP-MS analysis was determined by comparing the average bias between the experimentally obtained values and the reference values of the glass reference materials, and was found to be less than 10% for all reported elements. The reproducibility of the LA-ICP-MS analysis was determined by calculating the relative standard deviation (RSD) for the repeated analyses of the MPI-DING ATHO-G glass reference material. The reproducibility for most elements is <5% RSD, 5–10% RSD for Li, Ge, As, Mo, Cs, Tb and Tm, and <15% RSD for Be, Cr, Co, Ni, Sb and U. The reproducibility for the latter elements is likely related to their lower concentration (<12 ppm) in the ATHO-G reference glass, and is supported by their overall good reproducibility (<10% RSD) in other USGS and MPI-DING reference glasses, including BHVO-2G and ML3B-G.

The triple-oxygen isotope composition ($\delta^{17}O$, $\delta^{18}O$, $\Delta^{17}O$) of the achondritic cosmic spherules were determined using a Cameca IMS 1270 secondary ion mass spectrometer (SIMS) at the Centre de Recherches Pétrografiques et Géochimiques (CRPG, France). Oxygen isotopes were released from the sample surface by the incident Cs^+ ion beam at a 10–15° angle (spot size ca. 15 μm and ca. 2.5 nA beam current). The ions ($^{16}O^-$,$^{17}O^-$,$^{18}O^-$) were monitored simultaneously in multi-collection mode using Faraday cups. Samples were pre-sputtered and probed for 275 s with

Table 1
Overview of particle selections.

Particle	Size* (μm)	Colour	Weathering scale**
WF1801-AC1	341	n.o.	1a-b
WF1801-AC2	388	black	0a
WF1801-AC3	377	black/brown	1a-b
WF1801-AC4	526	n.o.	1a-b
WF1801-AC5	369	dark green/grey	1a-b

n.o.: The colour of this particle was not registered prior to analysis.
* The shape of the achondritic spherules was assumed to represent an oblate ellipsoid (a > b = c), where a is the longest axis and b and c are the shortest axes which have identical length. As such, the size of the achondritic spherules was estimated using the following formula: size (μm) = $(a \times b^2)^{(1/3)}$.
** van Ginneken et al. (2016).

between 4 and 7 spots averaged per analyzed particle (Table 2). To compensate for instrumental isotope fractionation effects, a total of three reference materials including the basaltic glass CLDR01, diopside JV1 and San Carlos olivine were measured five times at the start and end of each analysis session. Analytical uncertainties were determined based on repeated analysis of these three reference materials and found to be ±0.6‰ (2SE) for $\delta^{17}O$, ±0.6‰ (2SE) for $\delta^{18}O$ and ±0.6‰ (2SE) for $\Delta^{17}O$ on average over all analytical sessions and for all reference materials analysed, where SE stands for the standard error.

In-situ Fe isotope ratio measurements of the micrometeorites was performed using a ns-LA-MC-ICP-MS set-up using an Analyte G2 193 nm ArF*excimer-based LA-system (Teledyne Photon Machines Inc., Bozeman, MT, USA), equipped with a COBALT ablation cell and ARIS aerosol rapid introduction system (PEEK tubing with 1 mm ø) (Van Malderen et al., 2020), connected to a Thermo Scientific Neptune MC-ICP-MS instrument equipped with high-transmission interface and a Pfeiffer (Germany) OnTool™ Booster 150 dry interface pump (130 m^3 h^{-1} pumping speed) at Ghent University (Ghent, Belgium). Instrumental isotope fractionation correction relied on internal doping with a standard solution of Ni (500 ng mL^{-1}), continuously aspirated via pneumatic nebulizer and a double pass spray chamber, using a T-piece (5 mm ø) for mixing. The Fe isotope ratios were additionally corrected for potential drift by sample-standard bracketing (SSB) using the United States Geological Survey (USGS) basaltic glass reference material BCR-2G. The BCR-2G was ablated using a circular spot size of 15 µm diameter, laser energy density of 1.74 J cm^{-2} and a laser repetition rate of 20 Hz. To assure for an adequate correction relative to the reference material, the Fe intensities for the cosmic spherules were matched within 5% to those obtained for BCR-2G by adjusting the spot size (10–30 µm) and laser repetition rates (25–45 Hz). Nuclides at mass ^{53}Cr, $^{54}Fe + {}^{54}Cr$, ^{56}Fe, ^{57}Fe, $^{58}Fe + {}^{58}Ni$ and ^{60}Ni were measured simultaneously in an array of six Faraday cups at medium mass resolution ($m/\Delta m \sim 6000$). Chromium-53 was monitored to correct for the isobaric interference of ^{54}Cr on ^{54}Fe, applying the natural abundances of Cr. Further details of the method can be found in González de Vega et al. (2020a) and Lampe et al. (2022). The Fe isotope ratios of the CSs are expressed as δ-values relative to IRMM-014 international reference material, with $\delta^{i}Fe = [(^{i}Fe/^{54}Fe)_{sample}/(^{i}Fe/^{54}Fe)_{reference\ material} - 1] \cdot 1000$ (‰) (González de Vega et al., 2020b). Here ^{i}Fe represents the isotopes of interest i = 56, 57. Based on fifteen measurements in several separate analytical sessions of BCR-2G reference material, the intermediate precision (2SD) is 0.10‰ and 0.14‰ for $\delta^{56}Fe$ and $\delta^{57}Fe$, respectively. The internal precision for the individual cosmic spherules reported here varies between 0.12‰ and 0.22‰ for $\delta^{56}Fe$ and between 0.10‰ and 0.40‰ for $\delta^{57}Fe$ (2SE; Table 3).

3. RESULTS

3.1. Physical and petrographic properties

The achondritic cosmic spherules are relatively large and range in size between 341 and 526 µm (Table 1). These particles are classified as 'vitreous' following the classification of Genge et al. (2008) and display a variety of colors ranging from black, brown to dark green/grey. Particles often display palagonitization features as a result of terrestrial aqueous alteration processes (Fig. S1). Following the weathering scale defined by van Ginneken et al. (2016), particles WF1801-AC1, AC3, AC4 and AC5 classify as '1a-b' implying that a minor portion of the vitreous material was altered, and these particles possibly exhibit a surficial encrustation (see also Table 1). Particle WF1801-AC2 does not contain such alteration rim and classifies as '0a', indicating a lack of any significant alteration features.

3.2. Major element compositions

The achondritic nature of cosmic spherules was determined based on their distribution in Fe/Mg versus Fe/Mn space (Fig. 1). Four out of five particles reported here display Fe/Mg-Fe/Mn relations similar to or slightly below HED (Fe/Mn = 30 ± 2) and martian (Fe/Mn = 32 ± 6) meteorite reference values, but at widely varying Fe/Mg ratios (ca. 0.48–1.72). These values are comparable to the values determined for achondritic cosmic spherules from

Table 2
Oxygen isotope data of the Widerøefjellet achondritic spherules.

Particle	*n*	$\delta^{17}O$ (‰)	2SE (‰)	$\delta^{18}O$ (‰)	2SE (‰)	$\Delta^{17}O$ (‰)	2SE (‰)	R_0 (‰)	f	f*
WF1801-AC1	5	8.9	0.6	17.9	0.5	−0.5	0.6	3.6	0.45 (±0.01)	0.23 (±0.01)
WF1801-AC2	7	5.8		12.1		−0.5			0.30 (±0.01)	0.02 (±0.02)
WF1801-AC3	4	11.0		21.9		−0.4			0.53 (±0.01)	0.35 (±0.01)
WF1801-AC4	6	11.9		24.4		−0.8			0.58 (±0.01)	0.41 (±0.01)
WF1801-AC5	4	21.9		43.4		−0.7			0.81 (±0.00)	0.73 (±0.00)

We have calculated the fraction of oxygen that was presumably lost during atmospheric entry heating based on the Rayleigh fractionation law $R/R_0 = (1 - f)^{(1/\alpha - 1)}$, where R is the $\delta^{18}O$ composition of the cosmic spherule, R_0 is the $\delta^{18}O$ composition of a hypothetical parent body (here a bulk average value of 3.6 ± 0.4‰ (2SD) is taken based on a population of 7 monomict eucrites, 2 polymict eucrites, 2 cumulate eucrites, 7 diogenites, and 7 howardites; Greenwood et al., 2005), α is the isotopic fractionation factor (1.0237 – Wang et al., 2001), and *f* is the amount of oxygen that was lost as a result of evaporation/mass-dependent fractionation. We have also calculated f*, which represents the fraction of oxygen lost when the effects of atmospheric oxygen mixing (ca. 8‰, see Clayton et al. 1986; Lampe et al. 2022) are considered. *n* = number of spots for SIMS analysis.

Table 3
Iron and corrected oxygen isotope data of the Widerøefjellet achondritic spherules.

Particle	δ^{56}Fe (‰)	2SE (‰)	δ^{57}Fe (‰)	2SE (‰)	δ^{18}O (‰)	Δ^{17}O (‰)	Atmosphericmixing (‰)	δ^{18}O corrected* (‰)
WF1801-AC1	/	/	/	/	17.9	−0.5	8 (0/23.5)	9.9 (−5.6/17.9)
WF1801-AC2	0.43	0.14	0.71	0.24	12.1	−0.5		3.7 (−11.8/11.7)
WF1801-AC3	1.28	0.22	1.87	0.10	21.9	−0.4		12.6 (−2.9/20.6)
WF1801-AC4	11.53	0.12	17.19	0.40	24.4	−0.8		4.4 (−11.1/12.4)
WF1801-AC5	21.65	0.12	32.42	0.20	43.4	−0.7		12.8 (−2.7/20.8)

* The corrected value was calculated by compensating for mass-dependent fractionation processes following the equation $\delta^{18}O_{corr} = (\delta^{18}O_{meas} - 1.042 * \delta^{56}Fe_{meas}) - 8$, where $\delta^{18}O_{corr}$ is the δ^{18}O ratio corrected for mass-dependent fractionation effects, $\delta^{18}O_{meas}$ is the δ^{18}O ratio measured for the cosmic spherule, and $\delta^{56}Fe_{meas}$ is the δ^{56}Fe ratio measured in the cosmic spherule (Lampe et al., 2022). The uncertainty on the slope is not taken into account here, given the large uncertainties associated with atmospheric oxygen admixture (Fig. S2). An additional correction factor of 8‰ was subtracted to compensate for mixing processes with atmospheric oxygen following the observations by Clayton et al. (1986) and Lampe et al. (2022). The range given in between brackets covers no correction for atmospheric oxygen admixture (correction factor of 0‰) or complete oxygen isotope exchange (correction factor of 23.5‰ based on the δ^{18}O value for atmospheric oxygen; Thiemens et al., 1995). Since no Fe isotope data was acquired for particle WF1801-AC1, we have only applied the correction factor to compensate for mixing processes with atmospheric oxygen.

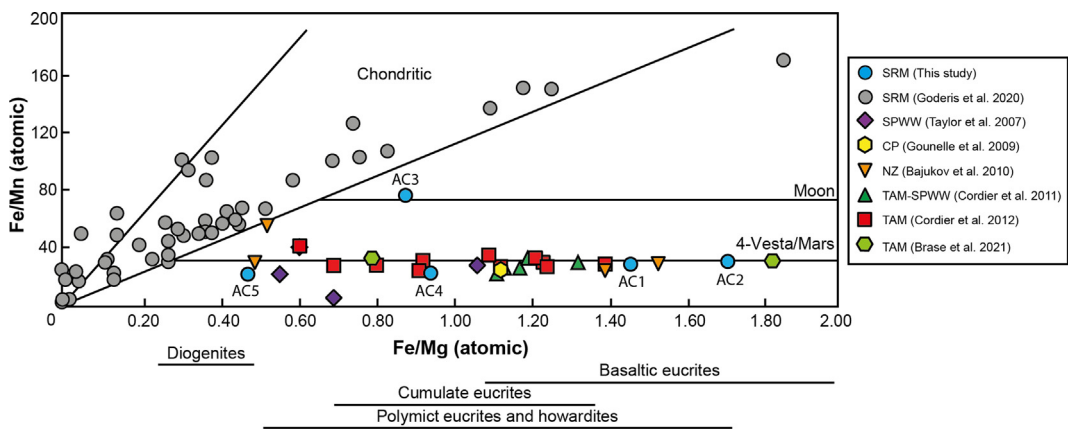

Fig. 1. Distribution of achondritic cosmic spherules in Fe-Mg-Mn space. Achondritic (micro)meteorites generally display higher Fe/Mg ratios at Fe/Mn ratios comparable to those of chondritic (micro)meteorites (grey circles). This can be attributed to a range of planetary scale differentiation processes. The vast majority of achondritic spherules is positioned along the 4-Vesta/Mars reference line, with the exception of particles NZ-6-2-4,5 (Badjukov et al. 2010) and WF1801-AC3. The latter particle displays a high Fe/Mn ratio of 78, comparable only to those of lunar rocks. In addition, the Fe/Mg ratios can provide approximate information regarding the precursor lithology (mantle versus crust). Reference values reproduced from Taylor et al. (2007), Gounelle et al. (2009), Badjukov et al. (2010), Cordier et al. (2011a, 2012), Goderis et al. (2020) and Brase et al. (2021). SRM – Sør Rondane Mountains, SPWW – South Pole Water Well, CP – Cap Prudhomme, NZ – Novaya Zemlya, TAM – Transantarctic Mountains. The data for micrometeorite 99-21-40 represents pyroxene data only (Gounelle et al. 2009).

the literature (Taylor et al., 2007; Cordier et al. 2011a, 2012; Brase et al., 2021), and are inconsistent with the distribution of chondritic cosmic spherules from the SRMs. The Fe/Mg ratios furthermore suggest that particles WF1801AC4 (Fe/Mg = 0.95) and WF1801-AC5 (Fe/Mg = 0.48) may potentially derive from more primitive, mantle-like precursor materials (e.g., diogenite, howardites, cumulate eucrites), whereas particles WF1801-AC1 (Fe/Mg = 1.47) and AC2 (Fe/Mg = 1.72) may have been inherited from a crustal-like (e.g., basaltic eucrite) precursor body. In contrast, particle WF1801-AC3 plots near the Fe/Mg ratios of WF18-AC4 and AC5, but at considerably higher Fe/Mn ratios (ca. 78), comparable only to values obtained for lunar rocks (Fe/Mn = 62 ± 18).

Achondritic spherules can also be distinguished from chondritic cosmic spherules (Goderis et al., 2020), microtektites (Soens et al., 2021) and meteoritic condensation debris (van Ginneken et al., 2021) previously recovered from the SRMs using the Si-Fe-Mg ternary diagram (Fig. 2). Achondritic spherules partly overlap in the 'chondritic micrometeorite' compositional field, but predominantly display elevated Si contents in comparison (Table S1). The Si content in achondritic spherules (SiO_2 = 40.9–54.1 wt%) is significantly lower than that observed in Australasian microtektites from the same Antarctic micrometeorite trap (SiO_2 = 66.4–76.1 wt%; Soens et al., 2021). Furthermore, Australasian microtektites tend to be enriched in K_2O (ca. 0.65–1.10 wt%). In contrast,

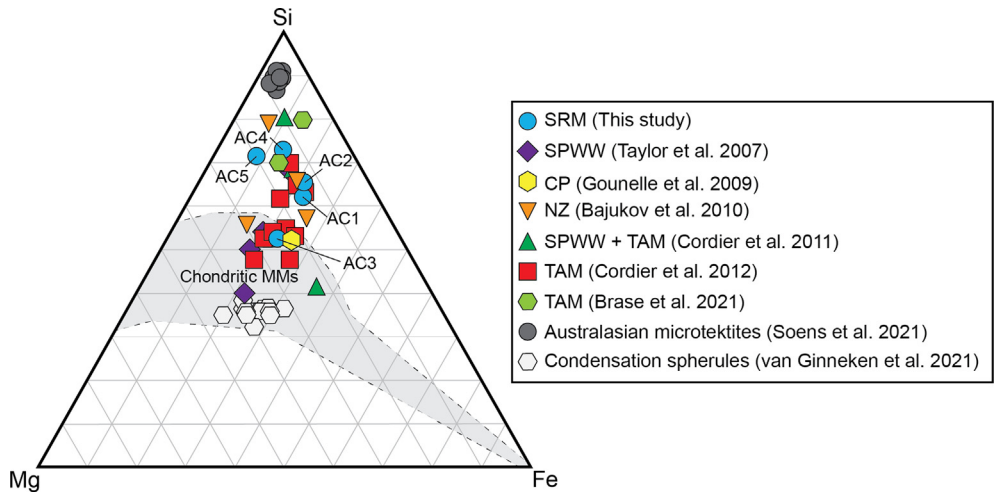

Fig. 2. Distribution of achondritic cosmic spherules in the Si-Fe-Mg ternary diagram. The compositional range of achondritic spherules partly overlaps with the compositional field of chondritic micrometeorites (Rochette et al., 2008). However, the majority of achondritic spherules display elevated Si contents compared to chondritic micrometeorites. Australasian microtektites previously recovered from the SRMs display significantly higher Si contents (Soens et al., 2021), while the meteoritic condensation spherules reported by van Ginneken et al. (2021) have lower Si contents and tend to be slightly more enriched in Mg. SRM – Sør Rondane Mountains, SPWW – South Pole Water Well, CP – Cap Prudhomme, NZ – Novaya Zemlya, TAM – Transantarctic Mountains. The data for micrometeorite 99-21-40 represents pyroxene only (Gounelle et al. 2009).

meteoritic condensation spherules are generally Si-poor (33.6–38.4 wt%) and enriched in Na_2O (ca. 0.26–1.34 wt %) and NiO (1.48–2.31 wt%) (van Ginneken et al., 2021).

Cordier et al. (2011b) have previously classified vitreous cosmic spherules into three distinct chemical classes, which are thought to reflect increasing degrees of volatilization experienced during atmospheric entry. This includes the 'normal chondritic', 'Ca-Al-Ti- or CAT-like' and 'high Ca-Al' subtypes. The bulk achondritic cosmic spherules reported here all plot within the 'high Ca-Al' field which is consistent with the majority (ca. 63%) of reference values from the literature (Fig. 3). The remaining particles (ca. 37%) plot within the 'normal chondritic' field at Fe/Si ratios above 0.30. No achondritic spherules plot within the 'CAT-like' field, which suggests that 'CAT-like' particles may have sampled a different type of precursor material and/or followed an evaporation regime distinct from most chondritic or achondritic micrometeorite precursor bodies. Furthermore, a rough trend can be observed that displays a negative correlation ($R2 = 0.72$) between the $CaO + Al_2O_3$ content and Fe/Si ratio of (mostly 'high Ca-Al') achondritic cosmic spherules, which may underline the importance of the precursor mineralogy on the bulk composition of differentiated cosmic spherules.

The former mineralogy of achondritic spherules can to some degree also be inferred based on their Ca/Si versus Al/Si systematics (Cordier et al., 2011a) (Fig. 4). The latter study observed Ca/Si and Al/Si atomic ratios ranging from 0.02–0.34 and 0.02–0.72, respectively. The achondritic spherules reported here display overall higher Ca/Si ratios (0.29–0.31), with particles WF1801-AC4 and WF1801-AC5 displaying values of 0.38 and 0.56, respectively. The Al/Si ratios are more consistent with the reference values for achondritic cosmic spherules and range from 0.02–0.70. Fig. 4 also displays the compositional fields of common mineral phases (e.g., pyroxene: low Al/Si ratio and low to moderately high Ca/Si ratio; plagioclase: high Al/Si ratio and moderately high Ca/Si ratio) observed in achondritic meteorites. Particles WF1801-AC1 and AC3 are located to the right of a cluster of reference values associated with cosmic spherules derived from basaltic eucrites. Particle WF1801-AC2 displays a chemical composition comparable to that of high-Ca pyroxene phases, and compatible with nakhlites (martian clinopyroxenites, consisting primarily of cumulus clinopyroxene and olivine; Udry and Day 2018). Particle WF1801-AC4 is slightly offset from the 'plagioclase' field and in close proximity to particle 3.5–7 from the TAM collection (Cordier et al., 2011a). Finally, particle WF1801-AC5 has a distinct composition, positioned away from the mineralogical fields and achondritic reference values with a Ca/Si of 0.56 and a moderately high Al/Si ratio of 0.40.

3.3. Trace element compositions

To further constrain the nature and mineralogy of the achondritic precursor bodies, we examine several key elements including the lithophile elements (e.g., Sr, Ba), siderophile-chalcophile elements (e.g., Co, Ni, V), and the REEs (Figs. 5 and 6). Strontium abundances are highly variable (8.10–163 μg/g) but lie within range (0.60–177 μg/g) of achondritic cosmic spherules previously analyzed by Cordier et al. (2011a, 2012) and Brase et al. (2021). Particles WF1801-AC1 and WF1801-AC3 are positioned close to a cluster of Type 1 (i.e., fine-grained eucrites consisting of pigeonite and anorthite) spherules, while particle WF1801-AC2 displays Sr abundances similar to those of Type 2–3 (i.e., pigeonite-rich eucrites and howardite-like

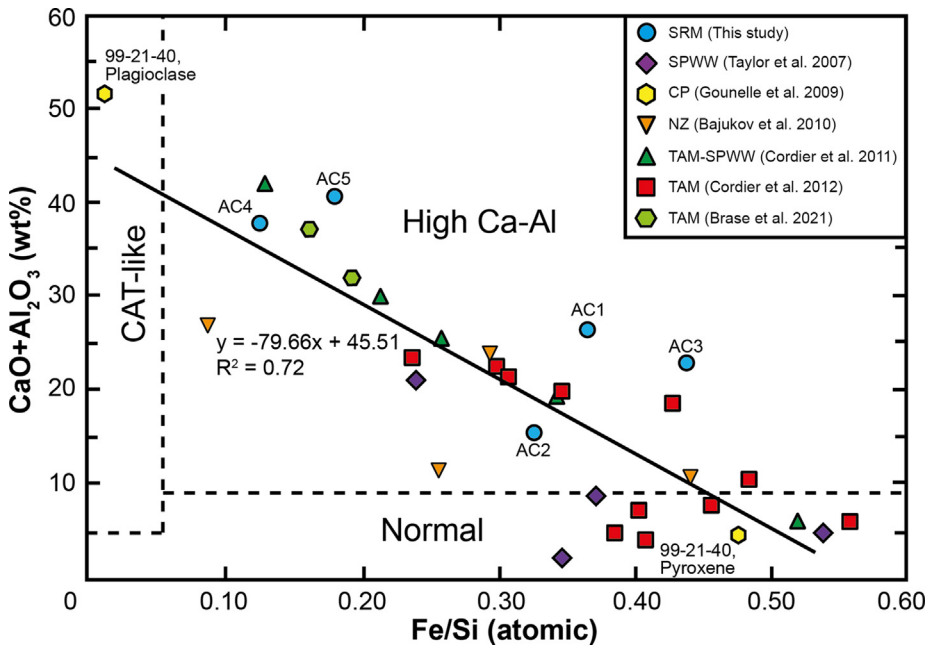

Fig. 3. Distribution of achondritic cosmic spherules in $CaO + Al_2O_3$ versus Fe/Si (atomic) space. Achondritic spherules are separated into two groups, i.e. 'normal chondritic' and 'high Ca-Al', based on the chemical classification scheme of Cordier et al. (2011b), which indicates the extent of evaporation experienced by micrometeorites during atmospheric entry heating on top of any mineralogical control. The majority ($n = 22$ or 71%) of bulk achondritic spherules are located within the 'high Ca-Al' field, while a smaller number ($n = 9$ or 29%) classify as 'normal chondritic'. This diagram suggests that the position of achondritic cosmic spherules is predominantly determined by their mineralogical precursors, as well as the total extent of volatilization during atmospheric entry heating. Reference values for achondritic spherules reproduced from Taylor et al. (2007), Gounelle et al. (2009), Badjukov et al. (2010), Cordier et al. (2011a, 2012) and Brase et al. (2021). The data for micrometeorite 99-21-40 represent both the pyroxene and plagioclase fractions as two separate data points (Gounelle et al. 2009).

precursor containing metal-bearing diogenite fragments) spherules but at a higher Fe/Mg ratio (Fig. 5A). The Sr concentration of particles WF1801-AC4 and WF1801-AC5 are elevated and match only the reference values reported for two particles in Brase et al. (2021) and a single particle in Cordier et al. (2011a).

Barium concentrations (Fig. 5B) appear to be more restricted (25.4–48.1 μg/g), except in the case of particle WF1801-AC2 that displays both depleted Sr and Ba (1.37 μg/g) abundances as observed in Type 2–3 spherules. Particles WF1801-AC1 and WF1801-AC3 fall close to the Type 1 cosmic spherule cluster. Analogous to Sr, particles WF1801-AC4 and WF1801-AC5 display elevated Ba contents.

Scandium concentrations in particles WF1801-AC1, WF1801-AC3 and WF1801-AC4 are fairly constant (34.6–39.0 μg/g) and consistent with Type 1 and Type 2 spherules (Fig. 5C). In contrast, Sc abundances in particles WF1801-AC2 (162 μg/g) and WF1801-AC5 (71.1 μg/g) are (markedly) higher and distinct from reference values from the literature.

Vanadium concentrations are highly variable (2.05–75.8 μg/g) for the particles measured here and positioned close to a cluster of achondritic cosmic spherules encompassing the three different types reported by Cordier et al. (2012), excepting particle WF1801-AC5. Typically, eucrites have lower V contents (76 ± 17 μg/g) than shergottites (206 ± 62 μg/g; Ruzicka et al. 2001) (Fig. 5D). Type 1 and Type 2 spherules and most other differentiated spherules previously reported in the literature share the characteristics of eucrites for this element (V < 100 μg/g; Cordier et al., 2012). Due to their pyroxene-rich precursors, Type 2 spherules have slightly higher V contents (up to 100 μg/g) than Type 1 spherules (<45 μg/g) and eucrites, but still below the values of shergottites, although atmospheric entry is known to affect both siderophile and chalcophile elements following high-density phase ejection (e.g., Cordier et al., 2011a; Goderis et al., 2020).

Nickel and cobalt are siderophile elements that are generally depleted in stony achondritic (micro)meteorites due to their accumulation and concentration in planetesimal or planetary cores. Most achondritic cosmic spherules studied here have low Ni abundances (3.12–10.7 μg/g), which is consistent with Type 1 and Type 2 reference values from literature. Particle WF1801-AC2 displays more elevated Ni concentrations (75.2 μg/g), comparable only to three particles from the SPWW-TAM collections described in Cordier et al. (2011a) and Cordier et al. (2012). A similar observation is made for the Co abundances of most particles studied here (<LOD–4.94 μg/g), which are compatible with Type 1–2 spherules. Particle WF1801-AC3 displays elevated Co concentrations (18.7 μg/g) comparable to a Type 1 particle reported by Cordier et al. (2011a) and below the values for two type 3 particles described in Cordier et al. (2012).

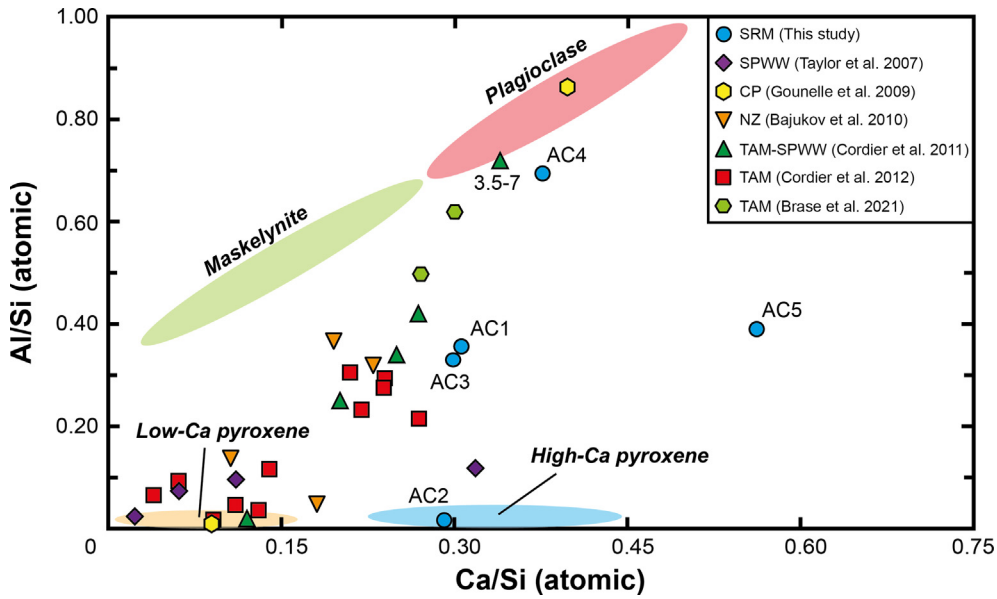

Fig. 4. Distribution of achondritic cosmic spherules in Al/Si versus Ca/Si space. The following diagram is useful to determine the mineralogical control on achondritic spherules. For instance, pyroxene phases have generally low Al/Si ratios, but their Ca/Si ratio may fluctuate depending on the pyroxene variety. Plagioclase is characterized by high Al/Si ratios and moderately high Ca/Si ratios. See text for further discussion. Reference values for plagioclase from Gooley (1972), Lovering (1975), Wilkening and Anders (1975), Gomes and Keil (1980), Floran et al. (1981), Fredriksson (1982), Christophe Michel-Levy et al. (1987), Mittlefehldt (1994), Metzler et al. (1995), Buchanan and Reid (1996), Cordier et al. (2011a). Reference values for maskelynite reproduced from Papike et al. (2009). Reference values for pyroxene from Lovering (1975), Harlow et al. (1979), Christophe Michel-Levy et al. (1987), Mittlefehldt and Lindstrom (1993), Mittlefehldt (1994), Fowler et al. (1994), Takeda et al. (1994), Pun and Papike (1995) and Cordier et al. (2011a). Reference values for achondritic spherules from Taylor et al. (2007), Gounelle et al. (2009), Badjukov et al. (2010), Cordier et al. (2011a, 2012) and Brase et al. (2021).

The REE pattern of V-type achondritic cosmic spherules is useful since the REEs in meteorite precursor materials mainly reside within accessory (rather than silicate) mineral phases, such as apatite and whitlockite (Harvey et al., 1993; Hsu and Crozaz, 1996), and the refractory nature of these elements leads to the overall preservation of the general REE pattern (except passive enrichment and, perhaps, Ce anomalies) of the precursor material despite atmospheric entry processes. The REE patterns for the achondritic cosmic spherules characterized here are presented in Fig. 6.

All achondritic spherules are highly enriched in the REE (average REE_N = 11.3–61.8, Eu excluded) with respect to chondritic (micro)meteorites. Particles WF1801-AC1 and WF1801-AC3 display relatively flat REE patterns ($(La/Yb)_N$ = 1.18–1.21) with minor, negative Eu anomalies (Eu* = 0.72–0.76) and are consistent with bulk eucrites and Type 1 spherules (Fig. 6A). While particle WF1801-AC3 displays Fe/Mn ratios comparable to lunar rocks (Fig. 1), its REE pattern is somewhat similar to that of Apollo basalts but considerably less enriched (Meyer, 2016).

Particle WF1801-AC2 displays a REE pattern similar to eucritic pigeonite/augite and Type 2 achondritic spherules, which are notably enriched in HREE with respect to the LREE ($(La/Yb)_N$ = 0.10) and exhibit a large, negative Eu anomaly (Eu* = 0.07; Fig. 6B). However, particle WF1801-AC2 is considerably more enriched in the REE (average REE_N = 29.9) relative to Type 2 achondritic spherules.

The REE pattern of particle WF1801-AC4 is broadly flat ($(La/Yb)_N$ = 0.93) but exhibits a large, positive Eu anomaly (Eu* = 2.56) and a small negative Ce anomaly, and cannot be linked to any known type of achondritic spherule and does not match the REE pattern of plagioclase (Fig. 6C). Yet, the contribution of plagioclase is clearly evidenced by its positive Eu-anomaly.

Finally, particle WF1801-AC5 displays the highest REE abundances (average REE_N = 61.8), is slightly enriched in LREE with respect to the HREE ($(La/Yb)_N$ = 1.59), and displays a moderately large, negative Eu anomaly (Eu* = 0.27; Fig. 6D). Particle WF1801-AC5 can thus not be linked to a known type of achondritic spherule, but its REE concentrations are matched only by those measured for Ca-phosphate (e.g., apatite, whitlockite) in (primitive) achondrites and the KREEP component of lunar basalts. However, unlike KREEP basalts, particle WF1801-AC5 only displays enriched Zr, Nb, Hf, REE, Ta and Th concentrations (Table S1). We have not observed achondritic cosmic spherules with REE patterns similar to the Type 3 differentiated cosmic spherules described in Cordier et al. (2012) during this study.

3.4. Oxygen isotope composition

The oxygen isotope data of the Widerøefjellet achondritic spherules displays a large range in $\delta^{17}O$ (5.8–21.9‰) and $\delta^{18}O$ (12.1–43.4‰) values, comparable to the range previously reported for $\delta^{17}O$ (7.0–10.0‰) and $\delta^{18}O$ (14.4–

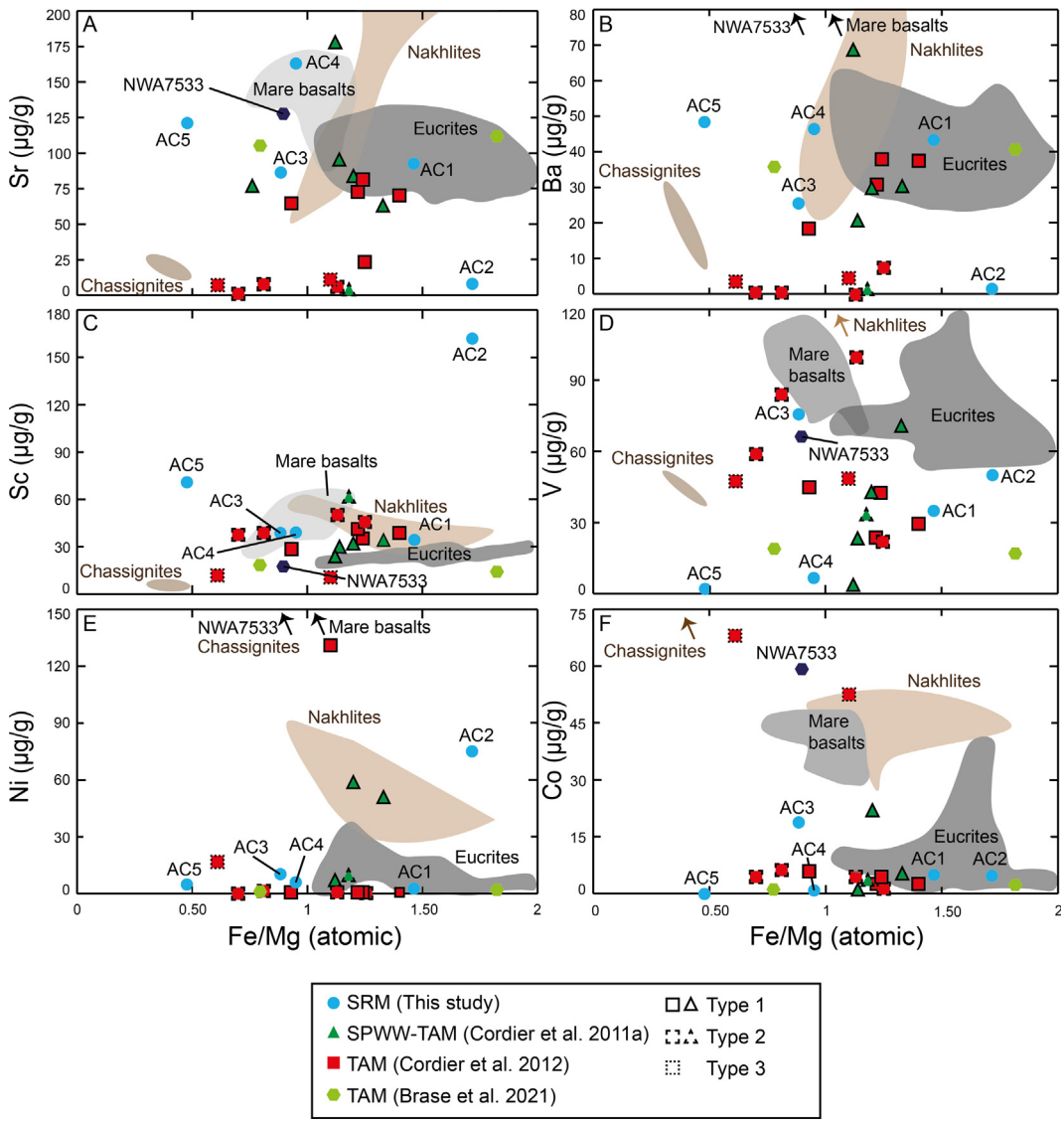

Fig. 5. Trace element compositions of the achondritic spherules. Reference values for 'eucrites' from McCarthy et al. (1973), Cleverly et al. (1986), Mittlefehldt and Lindstrom (1993, 2003), Kitts and Lodders (1998), Barrat et al. (2000, 2007), Buchanan et al. (2000), Patzer et al. (2003, 2005) and Yamaguchi et al. (2009). Reference values for 'mare basalts' from Haskin and Warren (1991). Reference value for nakhlites and chassignites from Udry and Day (2018). Reference values for NWA7533 (Martian regolith breccia) from Humayun et al. (2013). Reference values for trace elements in achondritic spherules from Taylor et al. (2007), Cordier et al. (2011a, 2012) and Brase et al. (2021).

20.1‰) by Cordier et al. (2012). The majority of SRM particles are positioned in close proximity of the TAM achondritic spherules ($\delta^{18}O$ of 12.1 to 24.4‰), except for particle WF1801-AC5 that displays a heavily fractionated oxygen isotope signature (Table 2, Fig. 7). In terms of $\Delta^{17}O$, all particles overlap, within uncertainty, with the oxygen isotope envelopes defined by the Eucrite (EFL) and Martian (MFL) fractionation lines, taking into account potential mass-dependent fractionation effects as the result of volatilization and mixing with atmospheric oxygen (Fig. 7). Note that all analyses were conducted on unaltered, fresh areas of the respective micrometeorite sections (Fig. S1). As such, we do not expect nor observe evidence for significant contributions of alteration products in equilibrium with Antarctic meteoric water and ice (Goderis et al., 2020).

3.5. Iron isotope composition

The iron isotope data record the effects of mass-dependent isotope fractionation (Table 3). This is demonstrated by data plotting within uncertainties along a mass-dependent fractionation line in the $\delta^{56}Fe$ - $\delta^{57}Fe$ space, which shows a positive correlation ($R^2 = 0.9977$) for S- and I-type cosmic spherules previously reported (Engrand et al., 2005; Pack et al., 2017; Lampe et al., 2022) (Fig. 8). For S-type cosmic spherules, Fe isotope fractionation appears to be negatively correlated with the FeO

abundance (Fig. 9). This correlation is not observed for I-type spherules. Furthermore, the extent of Fe evaporation and isotope fractionation for porphyritic (PO-type) and barred olivine (BO-type) spherules is not as pronounced as that observed for cryptocrystalline (C-type), vitreous (V-type) and CAT spherules, since the latter subtypes have endured higher peak temperatures and were thus subjected to higher degrees of thermal processing (e.g., Lampe et al., 2022). The V-type achondritic cosmic spherules measured here do not appear to follow this trend as particles WF1801-AC2 and WF1801-AC3 display similar values as BO spherules (δ^{56}Fe < 2‰; Table 3; Fig. 9). In contrast, particles WF1801-AC4 and WF1801-AC5 are heavily fractionated (δ^{56}Fe > 10 ‰), similar to many V-type and CAT spherules (Lampe et al., 2022).

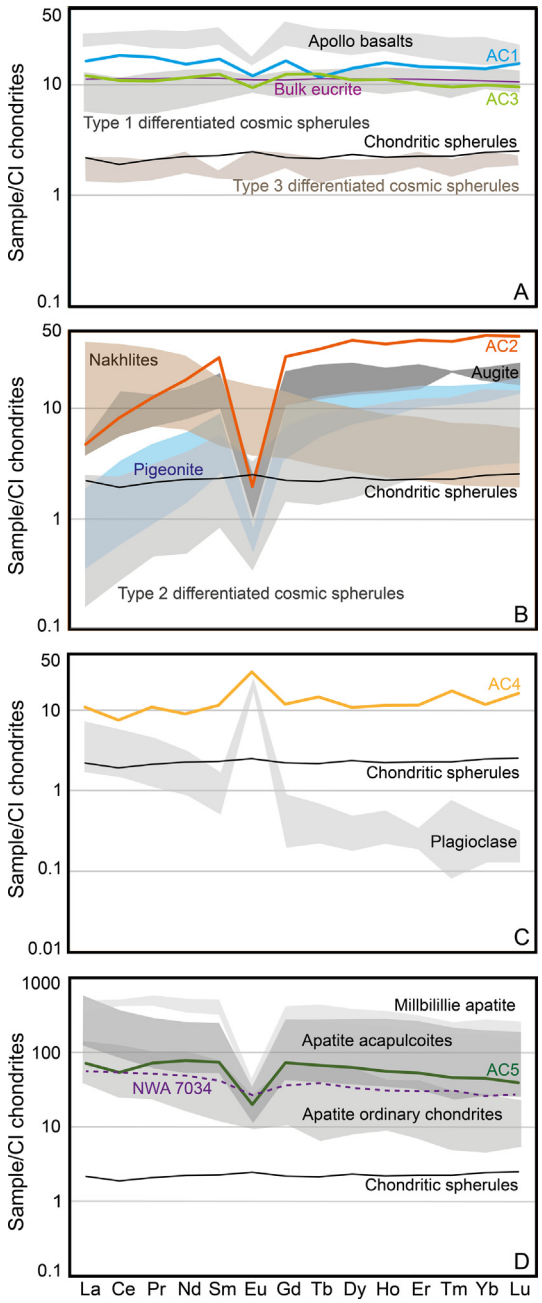

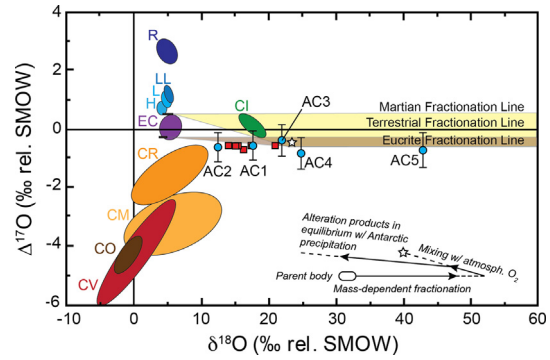

Fig. 7. Triple-oxygen (Δ^{17}O versus δ^{18}O) isotope diagram of achondritic cosmic spherules. All achondritic spherules overlap within uncertainty with the Eucrite Fractionation Line (Δ^{17}O = −0.242 ± 0.016‰ – Scott et al., 2009) and martian Fractionation Line (Δ^{17}O = 0.301 ± 0.013‰; Franchi et al., 1999). The oxygen isotopic composition of the atmosphere is for the transition from the stratosphere to the mesosphere (δ^{18}O ~ 23.5‰ and δ^{17}O ~ 11.8‰; Thiemens et al. (1995). Given the proximity of the original oxygen isotopic composition close to the TFL, admixing of atmospheric oxygen only has an incremental effect on the Δ^{17}O (see text for further explanation). Analytical uncertainty for TAM achondritic spherules is smaller than the symbol size. Plot adapted after Suavet et al. (2010). Reference values for TAM achondritic spherules are represented by the red square symbols and were reproduced from Cordier et al. (2012).

Fig. 6. Rare earth element pattern of achondritic cosmic spherules. The SRM particles have been separated into different diagrams depending on their REE pattern. We have also included the average REE pattern of 'normal chondritic' TAM cosmic spherules for comparison. A) Particles WF1801-AC1 and WF1801-AC3 have REE-enriched, but relatively flat patterns, similar to the Type 1 differentiated cosmic spherules reported by Cordier et al. (2012) and bulk eucrites (Kitts and Lodders, 1998; Barrat et al., 2007). Both particles display slightly negative Eu anomalies. Due to the compatibility of particle WF1801-AC3 with lunar basalts based on the Fe/Mn ratio (see Fig. 1), the REE pattern observed for Apollo basalts (Meyer, 2016) is included. B) Particle WF1801-AC2 displays a LREE-depleted and HREE-enriched pattern with a large Eu anomaly. This is comparable to the REE pattern of Type 2 differentiated cosmic spherules (Cordier et al., 2012), pigeonite and augite (Floss et al., 2000) in HED meteorites. This does not match the REE pattern of nakhlites (or chassignites; Treiman, 2005; Udry and Day, 2018) despite the similarity in Ca/Si and Al/Si ratios of particle WF1801-AC2. C) Particle WF1801-AC4 displays a roughly flat REE pattern with a moderately high, positive Eu anomaly. However, this does not match the LREE-enriched pattern of plagioclase from HED meteorites (Floss et al., 2000). D) Particle WF1801-AC5 displays a LREE-enriched pattern with a minor, negative Ce anomaly and a moderately large, negative Eu anomaly. Its pattern is not compatible with Type 1, Type 2 or Type 3 achondritic spherules, but strongly matches the KREEP component of mare basalts (Meyer, 2016), the REE signature of apatite in a variety of meteorite types (Crozaz et al., 1989; Ward et al., 2017) and the martian meteorite NWA 7034 (Agee et al., 2013). Normalization values for CI chondrites are from McDonough and Sun (1995).

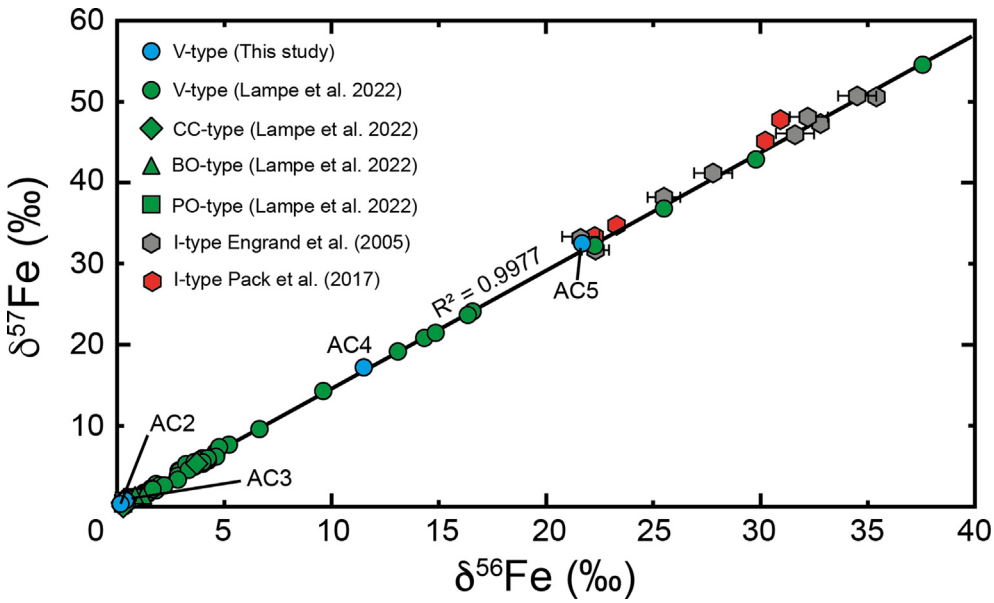

Fig. 8. Triple Fe-isotope diagram for S- and I-type spherules. The positive values along the mass-dependent fractionation line between the measured δ^{57}Fe and δ^{56}Fe ratios in cosmic spherules ($R^2 = 0.9977$) result from evaporation during atmospheric entry heating, as chondrites and differentiated planetary materials display fairly narrow ranges in δ^{56}Fe (±0.2‰ and ± 0.5‰, respectively) linked to a variety of kinetic and equilibrium processes (Johnson et al., 2021). The uncertainties for the δ^{56}Fe and δ^{57}Fe measurements are smaller than the symbol size used, unless otherwise indicated.

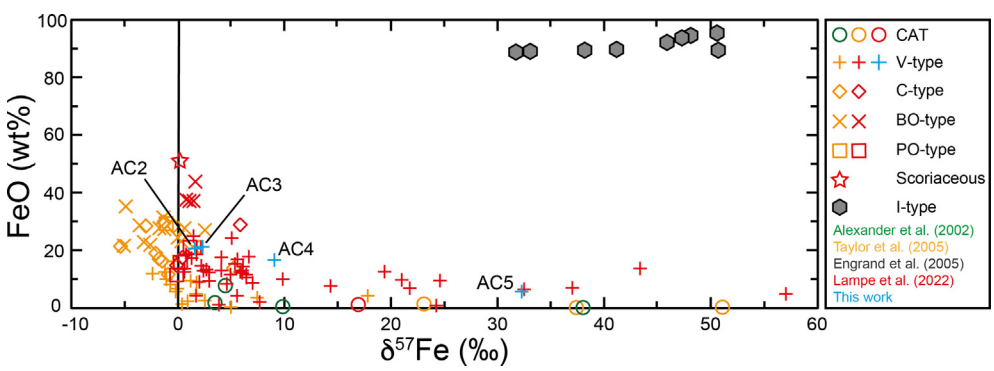

Fig. 9. FeO versus δ^{57}Fe diagram for S-type (chondritic and achondritic) and I-type spherules. The FeO content of S-type spherules roughly decreases as the δ^{57}Fe ratio increases. Additionally, the δ^{57}Fe ratio appears to increase for spherules displaying petrographic textures which reflect increasing heating temperatures (i.e., from PO-type over BO-type and C-type to V-type and CAT). This does not appear to be the case for the achondritic spherules (V-type, blue): particle WF1801-AC2 and particle WF1801-AC3 display vitreous textures but δ^{57}Fe ratios comparable to BO-type and C-type spherules. In contrast, particle WF1801-AC4 and particle WF1801-AC5 are heavily fractionated based on their δ^{57}Fe ratios. I-type spherules display similar FeO contents for varying degrees of iron isotope fractionation. The uncertainty is smaller than the symbol size.

4. DISCUSSION

4.1. Oxygen isotope ratios in cosmic spherules: A source of ambiguity

Oxygen isotope signatures can be used as a tracer to identify specific types of asteroidal or cometary bodies (e.g., Clayton, 1993; Clayton and Mayeda, 1996; Wiechert et al., 2004; Greenwood et al., 2005). To characterize the parent bodies of (achondritic) cosmic spherules, a thorough understanding of oxygen isotope systematics in micrometeorites is required. The oxygen isotope composition of cosmic spherules is generally not directly comparable to reference values for chondritic or achondritic meteorite groups (Yada et al., 2005; Suavet et al., 2010; Cordier et al., 2011b; Cordier et al., 2012; van Ginneken et al., 2017; Goderis et al., 2020; Rudraswami et al., 2020; Suttle et al., 2020; Soens et al., 2020). This can be attributed to mass-dependent fractionation of oxygen isotopes and mixing with atmospheric oxygen during atmospheric entry heating. Evaporation results in mass-dependent fractionation and a systematic increase of the abundances of heavier (^{17}O, ^{18}O) isotopes of oxygen compared to the lighter (^{16}O) isotope. This leads to a shift in the original oxygen isotope composition of a micrometeorite precursor body towards the right on a Δ^{17}O versus δ^{18}O diagram (Fig. 7). Additionally, atmospheric oxygen may be incorporated from the surrounding atmosphere during flash melting, which moves

the original oxygen isotope composition along a mixing line towards the stratospheric oxygen isotope value ($\delta^{18}O \approx 23.5‰$, $\delta^{17}O \approx 11.8‰$ – Thiemens et al., 1995). In the case of heavily altered particles, a shift towards lower $\delta^{18}O$ may also occur following the inclusion of alteration products in equilibrium with Antarctic precipitation (Goderis et al., 2020).

Cordier et al. (2012) previously attempted to compensate for the effects of atmospheric fractionation processes on achondritic cosmic spherules using oxygen isotopes alone based on two main assumptions. Firstly, the interaction with atmospheric oxygen was estimated to amount ca. 8‰ of $\delta^{18}O$ following the observations of Clayton et al. (1986) based on meteorite fusion crusts from meteorites. For simplicity, achondritic cosmic spherules were assumed to behave in a similar manner as such materials during atmospheric entry heating (Cordier et al. 2012). While CSs with a probable OC-like heritage have been shown to roughly exhibit a same degree of atmospheric mixing, increasing the $\delta^{18}O$ by ~5 to 10‰, data for a large set of glass cosmic spherules indicates such correction is not applicable to all S-type particles (Lampe et al., 2022). As there is a significant difference in the peak altitude of deceleration and the reaction with atmospheric gas between various particle types, corrections applying a constant value lead to considerable added uncertainty in the precursor identification, as further discussed in the sections below.

Secondly, the extent of mass-dependent fractionation was estimated based on reference values for oxygen isotope compositions of HED meteorites (i.e., $\delta^{18}O \approx 3.6‰$ – Greenwood et al., 2005) and the Rayleigh fractionation law $R/R_0 = (1 - f)^{(1/\alpha - 1)}$, where R is the $\delta^{18}O$ composition of the cosmic spherule, R_0 is the $\delta^{18}O$ composition of the parent body, α is the isotopic fractionation factor (1.0237 – Wang et al., 2001), and f is the amount of oxygen that was lost as a result of evaporation/mass-dependent fractionation. Based on these assumptions, Cordier et al. (2012) concluded that achondritic cosmic spherules have lost 10–30% ($f = 0.1$–0.3) of their oxygen due to evaporation when mixing with atmospheric oxygen is kept constant (i.e., a correction factor of 8‰ was applied). This fraction increases to ca. 30–50% ($f = 0.3$–0.5) when the latter process is not accounted for.

Applying this model to the oxygen isotope data of the Widerøefjellet achondritic spherules, we observe evaporation losses of between ~2 and 70% when we consider constant admixture of atmospheric oxygen (Table 2). These numbers increase to ca. 30–80% if we assume that mass-dependent fractionation was the sole process at play, which appears to be in line with the previous suggestion that mass fractionation due to heating dominates over the exchange with air in the case S-type particles (Rudraswami et al., 2020). It is important to emphasize that we have assumed a bulk eucrite precursor composition ($\delta^{18}O$ of 3.6 ± 0.4‰ , 2SD – Greenwood et al., 2005) and the variability within the HED parent body/ies affects these calculations only marginally (Table 2). As the model applied assumes a HED source, the results are evidently only valid for particles deriving from such precursors. Achondritic parent bodies displaying oxygen isotope compositions distinct from those measured for HED meteorites may consequently deviate to a large degree from these calculated values and will either underestimate or overestimate the extent of mass-dependent fractionation.

The calculated amount of oxygen that was lost as the result of evaporation is more limited for particles WF1801-AC1, WF1801-AC2, and WF1801-AC3 (~50% or less, and < 40% in the case the 8‰ correction factor is applied; Table 2), but more extensive in the case of particles WF1801-AC4 and WF1801-AC5 (ca. 60–80%, and ca. 40–70%, respectively). The latter are at the high end of those reported for stony chondritic particles ($f = 0.4 \pm 0.3$; Engrand et al., 2005) and those previously measured for achondritic spherules (see above – Cordier et al., 2012). This implies that at least particle WF1801-AC5 was subjected to extreme degrees of evaporation where the main fraction (>70%) of the original mass was lost. These large degrees of evaporation are supported by the Fe isotopic values of particles WF1801-AC4 and WF1801-AC5, and the major and trace element compositions may consequently also have been influenced to a large degree (cf. discussion below).

Meteorite fusion crusts are known to be roughly +0.35‰ heavier in $\delta^{56}Fe$ and accompanied by a 0.9–1.5‰ shift in towards heavier $\delta^{18}O$, because of evaporation during atmospheric passage and weathering (Hezel et al. 2015). Similar, albeit larger, isotope fractionations have been measured for silicate cosmic spherules (e.g., Alexander et al., 2002; Taylor et al., 2005; Lampe et al., 2022). To quantify the extent of mass-dependent oxygen isotope fractionation, Lampe et al. (2022) measured the oxygen ($\delta^{18}O$, $\delta^{17}O$, $\Delta^{17}O$) and iron ($\delta^{56}Fe$, $\delta^{57}Fe$) isotope composition for a set of chondritic cosmic spherules ($n = 36$; Fig. 10). They found that the $\delta^{18}O$ and $\delta^{57}Fe$ ratios of the CS, which experienced the largest degree of fractionation during atmospheric entry, covary according to the following empirical equation: $\delta^{18}O_{corr} = \delta^{18}O_{meas} - 1.042 \times \delta^{56}Fe_{meas}$, where $\delta^{18}O_{corr}$ is the $\delta^{18}O$ ratio corrected for mass-dependent fractionation effects, and $\delta^{18}O_{meas}$ and $\delta^{56}Fe_{meas}$ are the measured $\delta^{18}O$ and $\delta^{56}Fe$ ratios of the cosmic spherule (Fig. 10 and Fig. S2). The extent of mass-dependent fractionation in $\delta^{18}O$ based on the $\delta^{56}Fe_{meas}$ for the SRM achondritic spherules ranges from 0.4 to 22.6‰. This lies within the range reported by Lampe et al. (2022) for 36 V-type cosmic spherules (0.2–38.6‰ with an average of ca. 7.1 ± 9.0‰) (see Fig. 10).

This correction does not yet take into account potential effects of interaction with atmospheric oxygen. The admixture of atmospheric oxygen during transit through the atmosphere can vary from 0 to 23.5‰ based on the $\delta^{18}O$ value for atmospheric oxygen (Thiemens et al., 1995). While Cordier et al. (2012) assumed a constant $\delta^{18}O$ increase of ~8‰ (cf. discussion above), S-type particles, with the possible exception of OC material, have been shown to display a wider range of atmospheric oxygen admixture, which may be linked to the oxidation state of the precursor body or a differential response of the precursor mineralogy to atmospheric heating (Lampe et al., 2022). As such, here we report a range of corrected values, next to the commonly applied 8‰ correction (Table 3). The uncertainty associ-

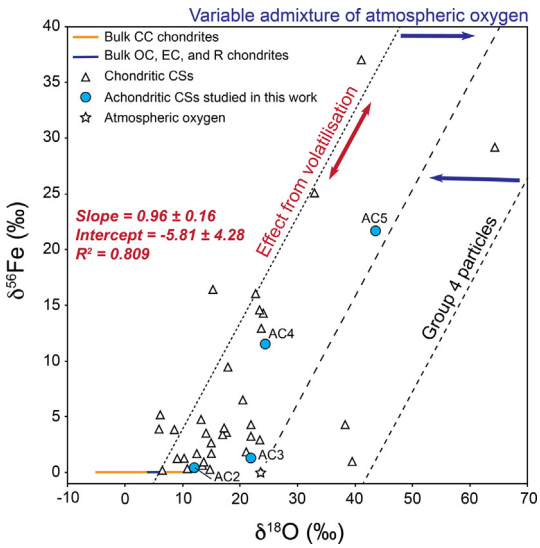

Fig. 10. Plot of δ^{56}Fe (in ‰) versus δ^{18}O (in ‰) based on Lampe et al. (2022). 'CC' indicates the initial δ^{18}O and δ^{56}Fe range of carbonaceous chondrites, while 'OC, EC, and R' shows the same initial ranges for ordinary chondrites, enstatite chondrites and Rumuruti chondrites. The calculation of the slope and intercept is explained in Fig. S2.

ated with the correction of mixing with atmospheric oxygen is considerably larger than that propagated from the calculated δ^{18}O - δ^{56}Fe regression (Fig. S2), which as a consequence is ignored in this discussion.

We can calculate the $\delta^{18}O_{corr}$* ratio as $\delta^{18}O_{corr}* = \delta^{18}O_{corr} - 8‰$, while the associated uncertainty is approximated by varying the atmospheric oxygen contribution between 0 and 23.5‰ (Table 3; Fig. 10). The calculated $\delta^{18}O_{corr}$* values for WF1801-AC2 and WF1801-AC4 of 3.7 (−11.8 to 11.7) ‰ and 4.4 (−11.1 to 12.4) ‰, respectively, cluster together, as do those for WF1801-AC3 and WF1801-AC5 with 12.6(−2.9 to 20.6) ‰ and 12.8(−2.7 to 20.8) ‰, respectively (Table 3). These obtained ranges, together with the distribution of the data in δ^{56}Fe - δ^{18}O space (Fig. 10), suggest that the 8‰ correction for atmospheric oxygen is inadequate in the case of particles WF1801-AC3 and WF1801-AC5, and require a δ^{18}O correction of +15–20‰ if derived from the same source material as WF1801-AC2 and WF1801-AC4. In this case, the oxidation state of the precursor material may have been distinct, or a distinct precursor mineralogy may need to be invoked. If these assumptions are correct, the exchange with atmospheric oxygen is more influential than mass-dependent fractionation due to heating in 50% of the particles. In the other two cases, mass fractionation due to evaporation dominates over exchange with atmospheric oxygen (Fig. 10).

While the current data set is small, it shows that cosmic spherules are characterized by distinct atmospheric entry histories in which the degrees of mixing and evaporation need to be evaluated on an individual basis (cf. discussion in Suavet et al. 2010; Rudraswami et al. 2020). In this context, the combined oxygen and iron isotope data can be used to unravel a particle's entry history. The exchange with the atmosphere and degree of mass-dependent fractionation due to heating are related to the entry angle and velocity of micrometeorites, as discussed by Suavet et al. (2010; 2011) and Rudraswami et al. (2020). Evaporation is mostly dependent on the peak temperature and duration of the heating pulse. The former increases with entry velocity or entry angle. At high velocity and high entry angle, particles experience higher peak temperatures and thus higher degrees of evaporation. Conversely, the duration of the heating pulse increases with decreasing entry angle. The time spent above the solidus has been shown to increase from 1–2 s at steep entry angles to > 12 s at shallow entry angles (Genge, 2017). Equally important is the chemistry and mineralogy of dust particles on atmospheric entry processes, as mass-dependent fractionation of oxygen may also be influenced by the presence of (moderately) volatile-rich precursors that undergo more partial evaporation than particles with refractory starting compositions (Genge and Grady, 1998; Rudraswami et al., 2020). Atmospheric entry processes may therefore be precursor and thus source-dependent, with the recorded atmospheric response linked to the primary physicochemical properties of the particle, such as a fine-grained versus coarse-grained or a volatile-rich versus refractory groundmass. Irrespective of the degree of atmospheric mixing used, two groups of particles (WF1801-AC2 and WF1801-AC4 versus WF1801-AC3 and WF1801-AC5) can be observed which display distinct $\delta^{18}O_{corr}$* ratios (Table 3 and Figs. 10, 11).

Importantly, based on an oxygen isotope survey of 137 cosmic spherules, the Δ^{17}O signatures of cosmic spherules appear to be mostly preserved, even while variations in $\delta^{17,\ 18}$O by evaporation can be large (Rudraswami et al., 2020). This is even more so the case for achondrite materials, as their O-isotope compositions tend to be relatively close to the TFL (<1‰ in Δ^{17}O, as in the case of lunar, HED, and martian materials). Mixing effects are therefore likely to have a small effect on the Δ^{17}O value and a larger effect on the δ^{18}O, especially when compared to the effects on carbonaceous chondrite precursors for example (Fig. 7; Suavet et al., 2010). Unfortunately, the Δ^{17}O ratios of most achondritic meteorites range from 0.32 to −0.26‰ (Clayton and Mayeda, 1996; Franchi et al., 1999) and require high-precision measurements, often preventing unambiguous assignment to specific achondrite parent bodies. This underlines the observations of Cordier et al. (2011a, 2012), who emphasized the importance of major and trace element chemistry in the identification of (a)chondritic precursor bodies in light of the ambiguity associated to oxygen isotope data. However, in the case of particles that have experienced extensive isotopic fractionation with a significant loss of mass (>40% of the oxygen lost), as observed for WF1801-AC4 and WF1801-AC5 based on their Fe isotopic composition (Table 3), their chemical composition may also have been affected severely.

In the following section, we attempt to characterize and identify the precursor body of the studied achondritic cosmic spherules based on their major, trace element chemistry (potentially linked to precursor mineralogy) and corrected oxygen isotope compositions, as calculated and discussed in the previous sections.

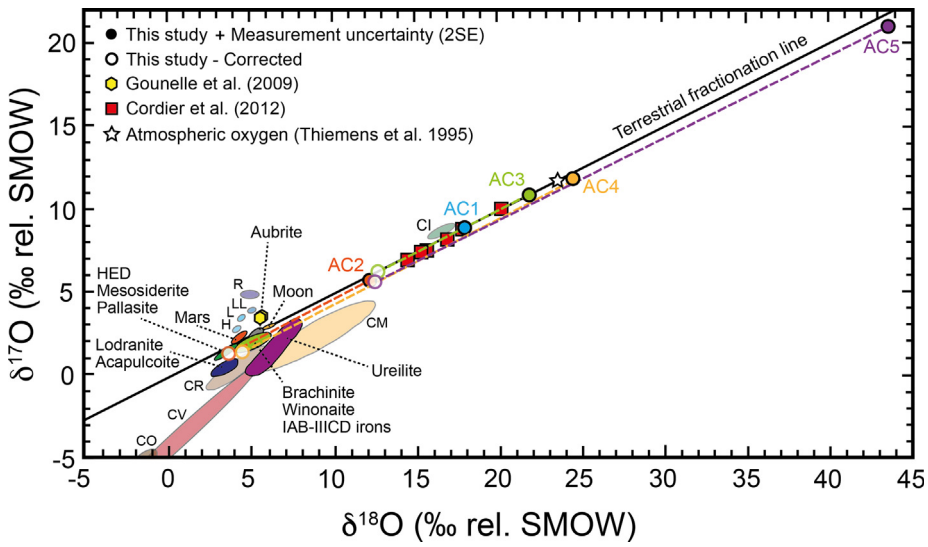

Fig. 11. Triple-oxygen ($\delta^{17}O$ versus $\delta^{18}O$) isotope diagram for achondritic micrometeorites. The measured oxygen isotope compositions are denoted by filled symbols, while the calculated oxygen isotope compositions are denoted by hollow symbols. Two particles (WF1801-AC2 and WF1801-AC4) show primary oxygen isotope compositions ($\delta^{18}O_{corr}$) comparable to HED meteorites and may thus originate from HED or HED-like parent bodies. The primary oxygen isotope compositions of particles WF1801-AC3 and WF1801-AC5 are not compatible with known (a)chondritic fields and may thus represent new types of achondritic parent bodies or indicate residual atmospheric entry effects.

4.2. Mineralogical control and parent body identification of the Widerøefjellet achondritic spherules

4.2.1. Particle WF1801-AC1

WF1801-AC1 is characterized by a $\Delta^{17}O$ of −0.5‰ (±0.6‰, 2SE), consistent with an achondritic origin, and a $\delta^{18}O$ of 17.9‰ (±0.5‰). Following the model described above, this particle may have lost up to 45% of its original oxygen (Table 2). The Fe isotopic composition of this particle was not determined.

The major element chemistry of particle WF1801-AC1 is consistent with a martian or HED-like parent body based on the Fe/Mn ratio of 30. Additionally, the relatively high Fe/Mg ratio (1.47) suggests that particle WF1801-AC1 may have sampled an evolved, basaltic-like precursor body, which developed from a significant degree of partial melting, such as basaltic/polymict eucrites or basaltic shergottites (Fig. 1). Both sources can be discriminated based on their bulk Al_2O_3 and Na contents as well as their Al_2O_3/CaO ratio. On average, eucrites display elevated Al_2O_3 contents (ca. 12 wt% versus 6.9 wt%) and Al_2O_3/CaO ratios (1.2 ± 0.1 wt% versus 0.8 ± 0.2 wt%) but are depleted in Na (0.5 ± 0.1 wt% versus 0.9 ± 0.4 wt%) compared to martian basalts (Basaltic Volcanism Study Project 1981; Lodders 1998; Jambon et al. 2002; Barrat et al. 2002; Mars Meteorite Compendium, 2003). Particle WF1801-AC1 has a high Al_2O_3 content of 13.8 wt% and intermediate Al_2O_3/CaO ratios (1.07), which are more compatible with a eucritic precursor body (Table S1). Due to the volatile nature of Na during atmospheric entry heating, the primary Na content cannot be constrained. Consequently, refractory elements including the REE, Ca and Al may have been passively enriched in the process. In addition, caution is required since the mineralogical abundance sampled by cosmic dust particles may not be representative of its precursor body. On the Ca/Si versus Al/Si diagram (Fig. 4), particle WF1801-AC1 is located to the upper right of a cluster of achondritic spherules, which have presumably sampled a fine-grained eucrite-like precursor body (Cordier et al., 2012). Potential deviations from this cluster could be attributed to the type and abundance of mineralogical precursors, as well as potential effects of volatilization during atmospheric entry heating. The position of particle WF1801-AC1 and the neighboring cluster of TAM achondritic spherules in the Ca/Si versus Al/Si diagram thus suggest that they sampled a plagioclase- and pyroxene-rich precursor body. Basaltic eucrites are predominantly composed of pigeonite and anorthite-rich plagioclase (An_{75-93}), but also contain minor amounts of chromite, ilmenite, silica, phosphate, Fe-Ni metal alloys, troilite and zircon (McSween et al., 2011). Basaltic eucrites are thus a likely precursor for particle WF1801-AC1.

The trace element composition of particle WF1801-AC1 is also consistent with eucrites, except for V which may reflect the effects of atmospheric entry under specific conditions (Fig. 5). The REE pattern of particle WF1801-AC1 (Fig. 6A) is roughly comparable albeit enriched relative to the Type 1 spherules reported by Cordier et al. (2012), which agrees with the observation that the particle was subjected to a moderate to higher degree of volatilization (Table 2). Type 1 spherules have previously been interpreted to derive from fine-grained (<1.5 mm in size) eucritic precursors predominantly consisting of pigeonite and plagioclase phases (Mittlefehldt et al., 1998; Cordier et al., 2012). Due to the lack of iron isotope data for particle WF1801-AC1, we were not able to fully compensate for oxygen isotope fractionation processes. However, based on its major and trace elemental chemistry, we propose that particle WF1801-AC1 was likely inherited from a fine-grained, eucritic precursor body.

4.2.2. Particle WF1801-AC2

WF1801-AC1 displays a $\Delta^{17}O$ of −0.5‰ (±0.6‰, 2SE) and a $\delta^{18}O$ of 12.1‰ (±0.5‰). Based on the measured $\delta^{56}Fe$ of 0.43‰ (±0.14‰, 2SE), this particle experienced limited evaporation during atmospheric entry, which translates to limited oxygen losses (Table 2, Fig. 11).

The major element composition of particle WF1801-AC2 is also consistent with a martian or HED-like parent body based on the Fe/Mn ratio of 32. However, unlike particle WF1801-AC1, this cosmic spherule is characterized by even higher Fe/Mg ratios (1.72), which is more consistent with basaltic eucrites or basaltic shergottites (Fig. 1). In addition, the Al_2O_3 contents (0.98 wt%) and Al_2O_3/CaO ratios (0.07) of this particle are relatively low and comparable to the values of nakhlites. This implies that the major element composition of particle WF1801-AC2 may have been predominantly controlled by high-Ca pyroxene phases such as pigeonite or augite (Fig. 4). Nakhlites, however, display considerably lower Fe/Mg ratios (ca. 0.92–1.08; Treiman, 2005; Udry and Day, 2018) in comparison to particle WF1801-AC2 and are therefore unlikely to represent its precursor body. In contrast, basaltic shergottites are predominantly composed of pyroxene phases (i.e., pigeonite and augite) and plagioclase (which is often transformed into glass or maskelynite due to shock metamorphosis), but commonly lack olivine (Stolper and McSween, 1979). The Mg numbers (Mg# = Mg/(Mg + Fe)*100) of basaltic shergottites are thus relatively low (Mg# = 23–52), which is consistent with that of particle WF1801-AC2 (Mg# of 37).

The pyroxene-rich nature of particle WF1801-AC2 is also evident from its trace element composition (Table S1, Fig. 5), where it displays relatively high Sc (162 μg/g), V (50.0 μg/g) and Cr (1462 μg/g) contents. Strontium (8.10 μg/g) and Ba (1.37 μg/g) concentrations are low relative to the other particles studied here (85.7–163 and 25.4–48.1 μg/g, respectively; Table S1) and indicate that the precursor was depleted in plagioclase. This is furthermore supported by the Eu contents of 0.11 μg/g and associated Eu* anomaly of 0.07, relative to values of 0.54–1.69 μg/g and 0.27–2.56 respectively for the other cosmic spherules. To discriminate the precursor body of particle WF1801-AC2, we can compare its siderophile (and to a lesser extent) chalcophile element (e.g., V, Cr, Co) contents with those of eucritic and martian basalts since for those meteorites the abundance of these elements is at least partly controlled by their oxygen fugacity levels during basalt petrogenesis, keeping in mind possible depletion following atmospheric entry. Righter and Drake (1996) suggested that the oxygen fugacity levels of martian basalts ($f(O_2) = -1.25$ ΔIW, where ΔIW represents the oxygen fugacity levels relative to the iron-wüstite buffer) are slightly higher than those of eucritic basalts ($f(O_2) = -2.2$ ΔIW), which implies that siderophile and chalcophile elements were more oxidized during the petrogenesis of basaltic shergottites. However, a recent study demonstrated that oxygen fugacity levels within shergottites vary considerably more than initially reported (i.e., $f(O_2) = -3.7$ to -0.2 ΔIW; Nicklas et al., 2021). Consequently, these elements tend to be more enriched in basaltic shergottites compared to basaltic eucrites. Cordier et al. (2011a, 2012) observed that V and Co contents remain largely unaltered during atmospheric entry heating and may thus to some extent be representative of their precursor material. As the isotopic signatures of this particle indicate limited evaporation during atmospheric entry and the Fe content is relatively high compared to the range observed in chondritic cosmic spherules (e.g., Goderis et al., 2020; Cordier et al., 2011b), implying metal beads likely did not form or segregate, a comparison of siderophile and chalcophile element contents reveals that particle WF1801-AC2 is more likely affiliated to basaltic eucrites than to shergottites (see Ruzicka et al., 2001).

The REE pattern of particle WF1801-AC2 is highly comparable to that of pigeonite and augite precursors from HED meteorites, and Type 2 differentiated cosmic spherules (Cordier et al., 2012), but is considerably more enriched, especially in the heavy REE (Fig. 6B). This signature is distinct from the REE pattern of nakhlite meteorites (Udry and Day, 2018). The corrected oxygen isotope composition of particle WF1801-AC2 is located within the HED meteorite field (Table 3, Fig. 10). Based on the combined set of criteria, particle WF1801-AC2 was thus likely inherited from a pigeonite- and/or augite-rich, basaltic eucrite precursor body.

4.2.3. Particle WF1801-AC3

WF1801-AC3 has a $\Delta^{17}O$ of −0.4‰ (±0.6‰, 2SE), overlapping the values determined for achondritic meteorites, and a $\delta^{18}O$ of 21.9‰ (±0.5‰). Based on the measured $\delta^{56}Fe$ of 1.28‰ (±0.22‰, 2SE), this particle experienced minor evaporation following atmospheric entry (Table 2). The position of this particle on the $\delta^{56}Fe$-$\delta^{18}O$ plot may indicate a large degree of atmospheric oxygen admixture (>70% assuming an HED-like origin and atmospheric oxygen $\delta^{18}O$ of 23.5‰; Figs. 10, 11).

Based on the distribution of various planetary materials in Fe/Mg versus Fe/Mn space (Fig. 1), particle WF1801-AC3 is consistent with values reported for lunar rocks. Lunar rocks have traditionally been classified into mare basalts and highland rocks, both of which predominantly consist of regolith breccias. Mare basalts fill up the lowerlying plains, originating from asteroidal or cometary impacts on the surface of the Moon. In general, mare basalts exhibit elevated FeO contents (>16 wt%), are relatively depleted in MgO and Al_2O_3, but are mostly characterized by highly variable TiO_2 contents (Haskin and Warren, 1991). As such, mare basalts are commonly distinguished based on their bulk TiO_2 content, which ranges from 'high-Ti' (>6 wt% TiO_2), 'medium-Ti' (1.5 wt% < TiO_2 < 6 wt%) and 'very-low-Ti' or 'VLT' (<1.5 wt% TiO_2). In addition, several compositional parameters including bulk Al_2O_3 (>11 wt%: 'aluminous' or 'high-Al') and K content (>2000 μg/g: 'high-K') are used to further classify mare basalts (Neal and Taylor, 1992). In comparison, highland rocks tend to be enriched in CaO (15.6 wt % on average) and Al_2O_3 (26.9 wt%), display higher Mg numbers (Mg# of 67) and have relatively low TiO_2 contents (0.37 wt%). Based on the abovementioned criteria, particle WF1801-AC3 appears to be more consistent with VLT mare basalts (FeO = 21.4 wt%, Al_2O_3 = 11.6 wt%, Mg# = 39, TiO_2 = 0.71 wt%), but does not match completely

since its FeO content is relatively high and the corresponding SiO_2 content is low (ca. 41 wt%). On the Ca/Si versus Al/Si diagram, particle WF1801-AC3 is positioned close to particle WF1801-AC1 (Fig. 4), which implies that the mineralogical precursors of particle WF1801-AC3 presumably also consisted of a mixture of plagioclase feldspar and pigeonite, similar to basaltic eucrites and mare basalts. Mare basalts mainly consist of pyroxene, plagioclase, olivine and minor oxide phases such as ilmenite and spinel (Papike et al., 1976), and could thus represent the precursor material of particle WF1801-AC3.

While certain trace element contents (e.g., Sc, V) in particle WF1801-AC3 plot within or close to the fields defined for lunar basalts, several of the lithophile and siderophile elements (e.g., Sr, Ba, Ni, Co) are clearly distinct (Fig. 5). The REE pattern of particle WF1801-AC3 is comparable to that of Type 1 achondritic spherules and fine-grained eucrites, supporting the pigeonite- and plagioclase-rich nature of the precursor material (Fig. 6A). While the Apollo basalts display a similar type of REE pattern, they tend to exhibit higher REE enrichments and a more pronounced negative Eu anomaly. The Eu anomalies in mare basalts are positively correlated with the level of REE enrichment and have been linked to parental materials that were cumulates in prior, perhaps primordial, differentiation that involved feldspar fractionation (Taylor et al., 1991; Longhi, 1992; Papike et al., 1998). While the REE abundances of particle WF1801-AC3 are relatively consistent with those of Apollo 17 and Luna 24 VLT mare basalt (2 to 10 × CI chondrite; Neal and Taylor, 1992), which can also display (slight) negative Eu anomalies, Apollo 17 VLT basalt have a slope in their REE patterns different from other lunar rocks with $(Lu/Yb)_N$ between 0.5 and 0.7. Luna 24 VLT mare basalts on the other hand have the bow shaped REE patterns characteristic of most mare basalts, while many contain positive Eu anomalies (Neal and Taylor, 1992).

As such, particle WF1801-AC3 is not compatible with any type of lunar basalt sampled to date based on its trace element chemistry. As the oxygen isotope composition of particle WF1801-AC3 may have been affected strongly by atmospheric admixture based on its position in Fe-O isotope space (Fig. 10), particle WF1801-AC3 cannot be assigned to any specific precursor material. While a lunar origin cannot be excluded, llunar and martian meteorites are ca. 20 times less abundant than HED meteorites, and the physicochemical properties (e.g., porosity, mechanical strength) of lunar rocks are not beneficial toward the production of lunar dust fragments within the micrometeorite population (Warren, 2001; Taylor et al., 2007). In summary, particle WF1801-AC3 sampled a (fine-grained?) precursor body, primarily composed of pyroxene and plagioclase, with Fe/Mn ratios similar to those of lunar rocks.

4.2.4. Particle WF1801-AC4

WF1801-AC4 has a $\Delta^{17}O$ of −0.8‰ (±0.6‰, 2SE), distinct from the terrestrial fractionation line (TFL), and a $\delta^{18}O$ of 24.4‰ (±0.5‰). Based on the measured $\delta^{56}Fe$ of 11.53‰ (±0.12‰, 2SE), this particle underwent moderately strong evaporation during atmospheric entry and exchange with atmospheric oxygen (Fig. 10), which translates to a loss of ~40% of its oxygen (Table 2, Fig. 11).

The Fe/Mg and Fe/Mn ratios of particle WF1801-AC4 are similar, but slightly lower, than those of HED and martian meteorites (Table S1, Fig. 1). The moderate degree of evaporation suggested by the measured Fe isotope ratios implies that the Fe/Mn and Fe/Mg ratios may have decreased as a consequence (Table 3). The interpretation of the Fe/Mg versus Fe/Mn systematics should thus be considered with care when the extent of iron isotope fractionation is significant. The Fe/Mg ratio suggests that particle WF1801-AC4 may have been inherited from cumulate/polymict eucrites and/or howardites. On the Ca/Si versus Al/Si diagram (Fig. 4), particle WF1801-AC4 is located slightly below the plagioclase (HED) field, implying a large contribution of this phase to its major element chemistry. This claim is supported by the position of this particle on the $CaO + Al_2O_3$ versus Fe/Si plot (Fig. 3).

In contrast, the trace element chemistry of particle WF1801-AC4 is not compatible with HED meteorites but may indicate a dependence on the type and abundance of minerals sampled (Fig. 5). The CI-normalized REE pattern of particle WF1801-AC4 is roughly flat and characterized by a moderately large, positive Eu anomaly and possibly a small, negative Ce anomaly (Fig. 6C). The positive Eu anomaly confirms the contribution of plagioclase to the major element chemistry of particle WF1801-AC4. Negative Ce anomalies have previously been observed in chondritic cosmic spherules, which have experienced large degrees of volatilization (i.e., 'CAT-like' and 'high Ca-Al' groups) (Cordier et al., 2011b; Goderis et al., 2020). This has been attributed to the volatile behaviour of Ce^{4+} within an oxidizing environment during non-equilibrium kinetic evaporation (Davis et al., 1982; Hashimoto, 1990; Floss et al., 1996; Wang et al., 2001), and has been reproduced by laboratory experiments (Floss et al., 1996; Wang et al., 2001). The REE signature of particle WF1801-AC4 is not consistent with the LREE-enriched pattern of plagioclase from HED meteorites, while the Eu anomaly of WF1801-AC4 is also less pronounced. This implies that additional (accessory) mineral phases were present to produce the REE pattern observed for particle WF1801-AC4.

The corrected oxygen isotope composition of particle WF1801-AC4 is positioned within the aubrite meteorite field, within relatively close proximity of the HED meteorite field (Table 3, Fig. 10). Consequently, particle WF1801-AC4 may have sampled a plagioclase-rich precursor body from HED-like asteroids.

4.2.5. Particle WF1801-AC5

WF1801-AC5 shows a $\Delta^{17}O$ of −0.7‰ (±0.6‰, 2SE), distinct from the TFL, with a $\delta^{18}O$ of 43.4‰ (±0.5‰; Table 2). The measured $\delta^{56}Fe$ of 21.65‰ (±0.12‰, 2SE) in combination with its oxygen isotopic compositions indicates that this particle experienced a high degree of evaporation during atmospheric entry, in excess of 70%, as well as a large exchange with atmospheric oxygen (Table 2; Figs. 10, 11).

WF1801-AC5 has the highest CaO and TiO_2 content of the characterized particles (CaO of 23.2 wt%, TiO_2 of 3.28

wt%), at moderate SiO_2 (44.0 wt%) and Al_2O_3 (14.8 wt%) and low FeO (6.65 wt%) concentrations. Based on its distribution in Fe/Mg versus Fe/Mn space (Fig. 1), particle WF1801-AC5 cannot be linked to HED, martian or lunar meteorites since its Fe/Mn ratio is relatively low (ca. 22). Note that, analogous to particle WF1801-AC4, the iron isotope composition of particle WF1801-AC5 is heavily fractionated and rivalled only by the most fractionated chondritic cosmic spherules (Table 2-3; Lampe et al., 2022), which may imply that the primary Fe/Mg and Fe/Mn ratios were (significantly) altered. Alternatively, particle WF1801-AC5 may have sampled an iron-poor precursor body or mineral phase. Particle WF1801-AC5 could also have sampled a primitive, mantle-like precursor body (e.g., diogenite), which could potentially explain the relatively high TiO_2 contents (3.28 wt%). Yet, given the extremely fractionated nature of particle WF1801-AC5 based on both its Fe and O isotope values, this may rather be a consequence of volatilization during atmospheric entry heating. On the Ca/Si versus Al/Si diagram (Fig. 4), particle WF1801-AC5 is positioned away from any mineralogical reference fields.

Given the extent of iron isotope fractionation, the primary Ca/Si and Al/Si ratios may have been lower as the respective equilibrium condensation temperatures are higher for Al (50% T_C = 1652–1653 K) and Ca (50% T_C = 1517–1535 K) relative to Si (50% T_C = 1310–1314 K) (Lodders, 2003; Wood et al., 2019). The larger difference between the 50% condensation temperatures of Al and Si suggests that the Al/Si ratio would increase more rapidly compared to the Ca/Si ratio. The primary position of particle WF1801-AC5 may thus have been below those of particles WF1801-AC1 and WF1801-AC3 or the high-Ca pyroxene field but cannot be constrained in detail following differential mineralogical responses to atmospheric heating.

The trace element composition of particle WF1801-AC5 is marked by a large enrichment of incompatible elements (e.g., Y, Zr, Nb, REE, Hf, Ta, Th) (Table S1). In contrast, the more volatile incompatible elements (e.g., Cs, Na_2O, K_2O) tend to be depleted, although this is not the case for Rb and Ba (Fig. 5). WF1801-AC5 has among the lowest siderophile and chalcophile element concentrations among the differentiated cosmic spherules characterized to date (Fig. 5).

Considering these observations, it is plausible that the enrichment of refractory, incompatible elements was at least in part caused by evaporation of (moderately) volatile elements during atmospheric entry heating. The REE pattern of particle WF1801-AC5 does not resemble reference values of achondritic spherules but resembles the pattern and enrichment levels observed for apatite from acapulcoites, ordinary chondrites, and the KREEP component of lunar rocks, with the exception of the minor, negative Ce anomaly (Fig. 6D). The KREEP component of lunar rocks mostly resides within Ca-phosphate mineral phases including apatite and whitlockite (Lucey et al., 2006). Consequently, the precursor material of particle WF1801-AC5 likely sampled a Ca-phosphate mineral phase, hosting the vast majority of REEs and superimposing the REE signature of any present silicate mineral phases. Ward et al. (2017) and Chernonozhkin et al. (2021) compiled refractory element ratios (Lu/Hf versus Sm/Nd) of phosphate minerals in a large variety of meteorites, which is useful here since the effects of volatilization and passive enrichment onto these refractory elemental ratios are largely negated. On a plot of Lu/Hf versus Sm/Nd, particle WF1801-AC5 with a Lu/Hf of 0.07 and Sm/Nd of 0.31 is located slightly below a cluster of basaltic achondrites, in proximity to all other differentiated cosmic spherules measured to date (Fig. S3). The corrected oxygen isotope composition of particle WF1801-AC5 is not located within a known meteorite field but plots relatively close to the corrected oxygen isotope composition of particle WF1801-AC3 (Fig. 10), implying residual atmospheric effects. As such, the precursor body of particle WF1801-AC5 cannot be constrained, most likely because of extreme volatilization, while a clear contribution of a Ca-phosphate mineral phase based on its REE signature is likely.

4.3. The abundance of achondritic cosmic spherules within the Widerøefjellet sedimentary trap

While several major and trace element concentrations and ratios, as well as O and Fe isotope signatures have been altered due to atmospheric processes, the combined use of several chemical and isotopic proxies (e.g., REE ratios, Fe/Mn versus Fe/Mg, and $\Delta^{17}O$) aids in reconstructing the origin of the particles studied here. A total of five achondritic cosmic spherules were identified in the Widerøefjellet sedimentary trap, which represents ca. 1–2% of all vitreous cosmic spherules and ca. 0.5% of all micrometeorites recovered to date. These numbers are comparable to those reported from other Antarctic micrometeorite collections, including the SPWW and TAM. For instance, Taylor et al. (2007) found that ca. 0.5 ± 0.4% of the SPWW micrometeorites could be affiliated to achondritic parent bodies, while Cordier et al. (2012) have reported a number of ca. 2.1% (of which 1.6% is related to 4-Vesta or vestoids) for achondritic micrometeorites from the TAMs. Finally, Badjukov et al. (2010) estimate that 0.45% of the micrometeorites recovered from the Novaya Zemlya glacier are basaltic in nature.

Similar to prior studies (Taylor et al., 2007; Badjukov et al., 2010; Cordier et al., 2011a, 2012), 3 out of the 5 differentiated particles studied here are consistent with HED-like mineralogy, Fe/Mn ratios and oxygen isotope ratios, with the chemical diversity linked to differential sampling of fine-grained basaltic eucrites, pigeonite-rich basaltic fragments, or diogenite clast-rich howardite fragments, deriving from the regolith of vestoid asteroids. Following the recommendation of previous studies, these spherules are referred to as HED-like rather than basaltic, to emphasize their derivation from differentiated vestoids, which may sample asteroids similar to but distinct from 4-Vesta (e.g., near-Earth vestoids; Burbine et al., 2009).

Out of 32 achondritic micrometeorites studied to date, 24 (75%) have been associated with vestoids with various degrees of confidence (Taylor et al., 2007; Gounelle et al., 2009; Badjukov et al., 2010; Cordier et al., 2011a, 2012; Brase et al., 2021). The remaining particles have tentatively

been linked to unknown (basaltic) precursors, Mars, or lunar mare basalts, although these identifications remain ambiguous following the chemical and isotopic modifications taking place during atmospheric entry. It needs to be noted that that trace element and isotopic proxies of the parent body origin of chondritic cosmic spherules (Lampe et al., 2022) are often decoupled from each other due to extreme evaporation during atmospheric entry and mineralogy effects. Owing to their low eutectic temperatures and small solidus to liquidus temperature intervals, differentiated achondrite materials are often more likely to melt than chondritic particles (Genge, 2017), which is reflected in the high proportion of cosmic spherules among the differentiated particles recovered to date.

The abundance of vestoid micrometeorites is similar to that of HED meteorites recovered from Antarctica, which produced the least biased collections of meteorites in the work (ca. 1.7%, http://www.lpi.usra.edu/meteor/metbull.php, accessed February 2022). The correspondence between micrometeorite and meteorite precursors that constitute the regolith of their differentiated parent body (Burbine et al., 2009) may suggest that the production and transport mechanisms of large (>1 mm) micrometeoroids and meteoroids may be similar. To leave their vestoid precursor body, the dust particles must have been accelerated to escape velocity during collisional events. Such events will also lead to higher entry velocities and a higher probability of melting upon atmospheric entry.

Future studies should place additional focus on non-vitreous type spherules since the texture of cosmic spherules is not solely determined by the composition of its precursor particle, but rather a combination of its physicochemical properties (e.g., chemical composition, density, size) and entry parameters (e.g., entry angle and velocity) (Love and Brownlee, 1991). While cosmic spherules are favored due to the small temperature interval of partial melting, the survival of unmelted grains at small sizes (<100 μm) remains possible (Genge, 2017), as evidenced by the recovery of achondritic micrometeorites as (partially) unmelted micrometeorites (e.g., Gounelle et al., 2009; Badjukov et al., 2010). In those cases, the micrometeorites may be so small that they sample a single mineral grain from their parent body, possibly reducing the potential to reliably constrain the particles' parent bodies (e.g., Taylor et al., 2012).

5. CONCLUSIONS

We present new major, trace element and oxygen isotope data for five vitreous achondritic cosmic spherules (341–526 μm) recovered from the Widerøefjellet sedimentary trap in the Sør Rondane Mountains (East Antarctica). This study also includes the first iron isotope data for four achondritic micrometeorites. Differentiated cosmic spherules were identified based on various chemical parameters, including their Fe/Mg versus Fe/Mn ratio, siderophile element contents (e.g., Co and Ni), and REE abundances and signatures. The data presented here extends the compositional ranges previously documented in achondritic micrometeorites from the SPWW and TAMs. The major, trace element and REE chemistry records both the mineralogical variety among achondritic micrometeorites as well as the degree of atmospheric entry heating. Our observations suggest that achondritic micrometeorites predominantly sample plagioclase- and/or pyroxene-rich precursor bodies such as basaltic achondrites, although accessory mineral phases (e.g., apatite) may also provide an important contribution with regards to the REE content. Atmospheric entry heating processes result in the volatilization of (moderately) volatile elements (e.g., Na, Cs, Si) and passively enrich more refractory elements (e.g., Zr, Hf, REE) in a manner similar to what is observed for chondritic micrometeorites.

The oxygen isotope composition of achondritic micrometeorites can often not be linked to precursor bodies due to oxygen isotope fractionation processes that take place following atmospheric entry, including mass-dependent fractionation and mixing with atmospheric oxygen. Based on this work, ~2 to 70% of the total oxygen content is lost due to mass-dependent fractionation processes assuming an initial oxygen isotope composition of bulk eucrite. To correct for these effects, we have measured and combined oxygen and iron isotope data following the observations by Lampe et al. (2022). The corrected oxygen isotope composition of two particles overlap with HED meteorites and could thus have sampled a HED(-like) precursor body. Yet, two particles could not be linked to a known type of achondritic precursor body and may have sampled a new type of asteroidal material or reflect residual atmospheric effects. This study thus supports previous observations, which argue that parent body identification of (a)chondritic parent bodies is only possible by combining major and trace elemental chemistry with (oxygen) isotopic information.

The abundance of achondritic micrometeorites (ca. 0.5%) in the Widerøefjellet sedimentary trap is comparable to that observed in the SPWW, TAM and Novaya Zemlya micrometeorite collections, emphasizing their rarity. The study of achondritic micrometeorites can represent valuable contribution to increase the inventory of materials from asteroidal and cometary bodies, and assist in refining their source region, within the Solar System.

Declaration of Competing Interest

The authors declare that they have no known competing financial interests or personal relationships that could have appeared to influence the work reported in this paper.

ACKNOWLEDGEMENTS

We like to thank Johan Villeneuve (CRPG) for his assistance during the SIMS measurement time. We would also thank the Research Foundation Flanders (FWO) for funding this PhD research to BS. SG, MvG, and PC acknowledge the support by the Belgian Science Policy (BELSPO) through BELAM, Amundsen and BAMM projects. SG, SCh and PC also thank the Research Foundation - Flanders (FWO – Vlaanderen), and the VUB strategic research. SG, PC, and FV acknowledge the support from the FWO–FNRS "Excellence of Science (EoS)" project ET–HoME (ID 30442502). CGdV acknowledges the grant received from the Marie Curie Clarin-COFUND project of the Principality of Asturias and the European Union. We thank Martin Suttle and 2 anony-

mous reviewers as well as associate editor James Day for their detailed comments and suggestions that significantly improved this manuscript.

APPENDIX A. SUPPLEMENTARY MATERIAL

The Supplementary Material file contains a table of the major and trace element data obtained using LA-ICP-MS, as well as backscatter electron-scanning electron microscope images (BSE-SEM) of four achondritic cosmic spherules, the calculation of the evaporation slope for δ^{56}Fe versus δ^{18}O, and a plot of Sm/Nd versus Lu/Hf for meteoritic materials.

Supplementary data to this article can be found online at https://doi.org/10.1016/j.gca.2022.03.029.

REFERENCES

Agee C. B., Wilson N. V., McCubbin F. M., Ziegler K., Polyak V. J., Sharp Z. D., Asmerom Y., Nunn M. H., Shaheen R., Thiemens M. H., Steele A., Fogel M. L., Bowden R., Glamoclija M., Zhang Z. and Elardo S. M. (2013) Unique meteorite from early Amazonian Mars: Water-rich basaltic breccia Northwest Africa 7034. *Science* **339**, 780–785.

Alexander C. M. O. D'., Taylor S., Delaney J. S., Ma P. and Herzog G. F. (2002) Mass-dependent fractionation of Mg, Si and Fe isotopes in five stony micrometeorites. *Geochim. Cosmochim. Acta* **66**, 173–183.

Badjukov D. D., Brandstätter F., Raitala J. and Kurat G. (2010) Basaltic micrometeorites from the Novaya Zemlya glacier. *Meteorit. Planet. Sci.* **45**, 1502–1512.

Barrat J., Blichert-Toft J., Gillet P. h. and Keller F. (2000) The differentiation of eucrites: The role of in situ crystallization. *Meteorit. Planet. Sci.* **35**, 1087–1100.

Barrat J. A., Jambon A., Bohn M., Gillet P. h., Sautter V., Göpel C., Lesourd M. and Keller F. (2002) Petrology and chemistry of the picritic shergottite Northwest Africa 1068 (NWA 1068). *Geochim. Cosmochim. Acta* **66**, 3505–3518.

Barrat J., Yamaguchi A., Greenwood R. C., Bohn M., Cotten J., Benoit M. and Franchi I. A. (2007) The Stannern trend eucrites: Contamination of main group eucritic magmas by crustal partial melts. *Geochim. Cosmochim. Acta* **71**, 4108–4124.

Basaltic Volcanism Study Project (1981) Petrology and chemistry of terrestrial, lunar and meteoritic basalts. In *Basaltic Volcanism on the Terrestrial Planets*. Pergamon Press, New York, pp. 214–235.

Bi D., Morton R. D. and Wang K. (1993) Cosmic nickel-iron alloy spherules from Pleistocene sediments, Alberta, Canada. *Geochim. Cosmochim. Acta* **57**, 4129–4136.

Brase L. E., Harvey R., Folco L., Suttle M. D., McIntosh E. C., Day J. M. D. and Corrigan C. M. (2021) Microtektites and glassy cosmic spherules from new sites in the Transantarctic Mountains, Antarctica. *Meteorit. Planet. Sci.* **56**, 829–843.

Brownlee D. E., Bates B. and Schram L. (1997) The elemental composition of stony cosmic spherules. *Meteorit. Planet. Sci.* **32**, 157–175.

Buchanan P. C. and Reid A. M. (1996) Petrology of the polymict eucrite Petersburg. *Geochim. Cosmochim. Acta* **60**, 135–146.

Buchanan P. C., Mittlefehldt D. W., Hutchison R., Koeberl C., Lindstrom D. J. and Pandit M. K. (2000) Petrology of the Indian eucrite Piplia Kalan. *Meteorit. Planet. Sci.* **35**, 609–616.

Burbine T. H., Buchanan P. C., Dolkar T. and Binzel R. P. (2009) Pyroxene mineralogies of near-Earth vestoids. *Meteorit. Planet. Sci.* **44**, 1331–1341.

Chernonozhkin S. M., McKibbin S. J., Goderis S., Van Malderen S. J. M., Claeys P. h. and Vanhaecke F. (2021) New constraints on the formation of main group pallasites derived from *in situ* trace element analysis and 2D mapping of olivine and phosphate. *Chem. Geol.* **562**, 119996.

Christiansen E. H., Best M. G. and Radebaugh J. (2022) The origin of magma on planetary bodies. In *Comparative Planetology, Planetary Volcanism across the Solar System* (eds. T. K. P. Gregg, R. M. C. Lopes and S. A. Fagents). Elsevier, pp. 235–270.

Christophe Michel-Levy M., Bourot-Denise M., Palme H., Spettel B. and Wänke H. (1987) L'eucrite de Bouvante: chimie, pétrologie et minéralogie. *Bull. Minéral.* **110**, 449–458.

Clayton R. N. (1993) Oxygen isotopes in meteorites. *Annu. Rev. Earth Planet. Sci.* **21**, 115–149.

Clayton R. N. and Mayeda T. K. (1996) Oxygen-isotope studies of achondrites. *Geochim. Cosmochim. Acta* **60**, 1999–2018.

Clayton R. N., Mayeda T. K. and Brownlee D. E. (1986) Oxygen isotopes in deep-sea spherules. *Earth Planet. Sci. Lett.* **79**, 235–240.

Cleverly W. H., Jarosewich E. and Mason B. (1986) Camel Donga meteorite – a new eucrite from the Nullarbor Plain, Western Australia. *Meteoritics* **21**, 263–269.

Cordier C., Folco L. and Taylor S. (2011a) Vestoid cosmic spherules from the South Pole Water Well and Transantarctic Mountains (Antarctica): a major and trace element study. *Geochim. Cosmochim. Acta* **75**, 1199–1215.

Cordier C., Folco L., Suavet C., Sonzogni C. and Rochette P. (2011b) Major, trace element and oxygen isotope study of glass cosmic spherules of chondritic composition: The record of their source material and atmospheric entry heating. *Geochim Cosmochim. Acta* **75**, 5203–5218.

Cordier C., Suavet C., Folco L., Rochette P. and Sonzogni C. (2012) HED-like cosmic spherules from the Transantarctic Mountains, Antarctica: Major and trace element abundances and oxygen isotopic compositions. *Geochim. Cosmochim. Acta* **77**, 515–529.

Crozaz G., Pellas P., Bourot-Denise M., de Chazal S. M., Fiéni C., Lundberg L. L. and Zinner E. (1989) Plutonium, uranium, and rare earths in the phosphates of ordinary chondrites – The quest for a chronometer. *Earth Planet. Sci. Lett.* **93**, 157–169.

Davis A. M., Tanaka T., Grossman L., Lee T. and Wasserburg G. J. (1982) Chemical composition of HAL, an isotopically-unusual Allende inclusion. *Geochim. Cosmochim. Acta* **46**, 1627–1651.

Duke J. M. (1976) Distribution of the period four transition elements among olivine, calcic pyroxene, and mafic silicate liquid: Experimental results. *J. Petrol.* **17**, 499–521.

Duprat J., Dobrică E., Engrand C., Aléon J., Marrochi Y., Mostefaoui S., Meibom A., Leroux H., Rouzaud J.-N., Gounelle M. and Robert F. (2010) Extreme deuterium excesses in ultracarbonaceous micrometeorites from Central Antarctic Snow. *Science* **328**, 742–745.

Engrand C. and Maurette M. (1998) Carbonaceous micrometeorites from Antarctica. *Meteorit. Planet. Sci.* **33**, 565–580.

Engrand C., McKeegan K. D., Leshin L. A., Herzog G. F., Schnabel C., Nyquist L. E. and Brownlee D. E. (2005) Isotopic compositions of oxygen, iron, chromium and nickel in cosmic spherules: Toward a better comprehension of atmospheric entry heating effects. *Geochim. Cosmochim. Acta* **69**, 5365–5385.

Floran R. J., Prinz M., Hlava P. F., Keil K., Spettel B. and Wänke H. (1981) Mineralogy, petrology, and trace element geochemistry of the Johnstown meteorite: a brecciated orthopyroxenite with siderophile and REE-rich components. *Geochim. Cosmochim. Acta* **45**, 2385–2391.

Floss C., Goresy A. E., Zinner E., Kransel G., Rammensee W. and Palme H. (1996) Elemental and isotopic fractionations produced through evaporation of the Allende CV chondrite: implications for the origin of HAL-type hibonite inclusions. *Geochim. Cosmochim. Acta* **60**, 1975–1997.

Floss C., Crozaz G., Yamaguchi A. and Keil K. (2000) Trace element constraints on the origins of highly metamorphosed Antarctic eucrites. *Antarct. Meteorite Res.* **13**, 222–237.

Folco L. and Cordier C. (2015) Micrometeorites. In *EMU Notes in Mineralogy 15: Planetary Mineralogy* (eds. M. R. Lee and H. Leroux). European Mineralogical Union, Twickenham, United Kingdom, pp. 253–297.

Fowler G. W., Papike J. J., Spilde M. N. and Shearer C. K. (1994) Diogenites as asteroidal cumulates: Insights from orthopyroxene major and minor element chemistry. *Geochim. Cosmochim. Acta* **58**, 3921–3929.

Franchi I. A., Wright I. P., Sexton A. S. and Pillinger C. T. (1999) The oxygen-isotopic composition of Earth and Mars. *Meteorit. Planet. Sci.* **34**, 657–661.

Fredriksson K. (1982) The Manegaon diogenite. *Meteoritics* **17**, 141–144.

Genge M. J. (2017) The entry heating and abundances of basaltic micrometeorites. *Meteorit. Planet. Sci.* **52**, 1000–1013.

Genge M. J. and Grady M. M. (1998) Melted micrometeorites from Antarctic ice with evidence for the separation of immiscible Fe-Ni-S liquids during entry heating. *Meteorit. Planet. Sci.* **33**, 425–434.

Genge M. J. and Grady M. M. (1999) The fusion crust of stony meteorites: Implications for the atmospheric reprocessing of extraterrestrial materials. *Meteorit. Planet. Sci.* **34**, 341–356.

Genge M. J., Engrand C., Gounelle M. and Taylor S. (2008) The classification of micrometeorites. *Meteorit. Planet. Sci.* **43**, 497–515.

Goderis S., Soens B., Huber M. S., McKibbin S., van Ginneken M., Debaille V., Greenwood R. C., Franchi I. A., Cnudde V., Van Malderen S., Vanhaecke F., Koeberl C., Topa D. and Claeys P. h. (2020) Cosmic spherules from Widerøfjellet, Sør Rondane Mountains (East Antarctica). *Geochim. Cosmochim. Acta* **270**, 112–143.

Gomes C. B. and Keil K. (1980) *Brazilian Stone Meteorites*. Univ. New Mexico Press, Albuquerque, p. 162.

González de Vega C., Chernonozhkin S. M., Grigoryan R., Costas-Rodriguez M. and Vanhaecke F. (2020a) Characterization of the new isotopic reference materials IRMM-524A and ERM-AE143 for Fe and Mg isotopic analysis of geological and biological samples. *J. Anal. At. Spectrom.* **35**, 2517–2529.

González de Vega C., Costas-Rodriguez M., Van Acker T., Goderis S. and Vanhaecke F. (2020b) Nanosecond laser ablation – multicollector inductively coupled plasma – mass spectrometry for in-situ Fe isotopic analysis of micrometeorites: Application to micrometer-sized glassy cosmic spherules. *Anal. Chem.* **92**, 3572–3580.

Goodrich C. A. and Delaney J. S. (2000) Fe/Mg-Fe/Mn relations of meteorites and primary heterogeneity of primitive achondrite parent bodies. *Geochim. Cosmochim. Acta* **64**, 149–160.

Gooley R. (1972) *The Chemistry and Mineralogy of Diogenites*. Arizona State University, Ph.D. thesis.

Gounelle M., Chaussidon M., Morbidelli A., Barrat J.-A., Engrand C., Zolensky M. E. and McKeegan K. D. (2009) A unique basaltic micrometeorite expands the inventory of solar system planetary crusts. *Proc. Natl. Acad. Sci. U.S.A.* **106**, 6904–6909.

Greenwood R. C., Franchi I. A., Jambon A. and Buchanan P. C. (2005) Widespread magma oceans on asteroidal bodies in the early Solar System. *Nature* **435**, 916–918.

Greenwood R. C., Burbine T. H., Miller M. F. and Franchi I. A. (2017) Melting and differentiation of early-formed asteroids: the perspective from high precision oxygen isotope studies. *Chemie der Erde-Geochem.* **77**, 1–43.

Harlow G. E., Nehru C. E., Prinz M., Taylor G. J. and Keil K. (1979) Pyroxenes in Serra de Magé: Cooling history in comparison with Moama and Moore County. *Earth Planet. Sci. Lett.* **43**, 173–181.

Harvey R. P., Wadhwa M., McSween H. Y. and Croraz G. (1993) Petrography, mineral chemistry, and petrogenesis of Antarctic shergottite LEW88516. *Geochim. Cosmochim. Acta* **57**, 4769–4783.

Hashimoto A. (1990) Evaporation kinetics of forsterite and implications for the early solar nebula. *Nature* **347**, 53–55.

Haskin L. and Warren P. (1991) Chapter 8: Lunar Chemistry. In *Lunar Sourcebook: A User's Guide to the Moon* (eds. G. Heiken, D. Vaniman and B. M. French). Cambridge University Press, Cambridge, pp. 357–474.

Hezel D. C., Poole G. M., Hoyes J., Coles B. J., Unsworth C., Albrecht N., Smith C., Rehkämper M., Pack A., Genge M. and Russell S. S. (2015) Fe and O isotope composition of meteorite fusion crusts: Possible natural analogues to chondrule formation? *Meteorit. Planet. Sci.* **50**, 229–243.

Hsu W. and Crozaz G. (1996) Mineral chemistry and the petrogenesis of eucrites: I. Noncumulate eucrites. *Geochim. Cosmochim. Acta* **60**, 4571–4591.

Hublet G., Debaille V., Wimpenny J. and Yin Q.-Z. (2017) Differentiation and magmatic activity in Vesta evidenced by ^{26}Al-^{26}Mg dating in eucrites and diogenites. *Geochim. Cosmochim. Acta* **281**, 73–97.

Humayun M., Nemchin A., Zanda B., Hewins R. H., Grange M., Kennedy A., Lorand J.-P., Göpel C., Fieni C., Pont S. and Deldicque D. (2013) Origin and age of the earliest Martian crust from meteorite NWA 7533. *Nature* **503**, 513–516.

Jambon A., Barrat J. A., Sautter V., Gillet P, Göpel C., Javoy M., Joron J.-L. and Lesourd M. (2002) The basaltic shergottite Northwest Africa 856: Petrology and chemistry. *Meteorit. Planet. Sci.* **37**, 1147–1164.

Johnson C., Beard B. and Weyer S. (2021) Iron geochemistry: an isotopic perspective. In *Advances in Isotope Geochemistry* (ed. J. Hoefs). Springer Nature, Switzerland, p. 360.

Kamei A., Horie K., Owada M., Yuhara M., Nakano N., Osanai Y., Adachi T., Hara Y., Terao S., Teuchi T., Shimura T., Tsukada K., Hokada T., Iwata C., Shiraishi K., Ishizuka H. and Takahashi Y. (2013) Late Proterozoic juvenile arc metatonalite and adakitic intrusions in the Sør Rondane Mountains, eastern Dronning Maud Land, Antarctica. *Precambrian Res.* **234**, 47–62.

Kitts K. and Lodders K. (1998) Survey and evaluation of eucrite bulk compositions. *Meteorit. Planet. Sci.* **33**, A197–A213.

Kojima S. and Shiraishi K. (1986) Note on the geology of the western part of the Sør Rondane Mountains, East Antarctica. *Mem. Natl. Inst. Polar Res.* **43**, 116–131.

Kurat G., Koeberl C., Presper T., Brandstätter F. and Maurette M. (1994) Petrology and geochemistry of Antarctic micrometeorites. *Geochim. Cosmochim. Acta* **58**, 3879–3904.

Lampe S., Soens B., Chernonozkhin S. M., González de Vega C., van Ginneken M., Van Maldeghem F., Vanhaecke F., Glass B. P., Franchi I. A., Debaille V., Claeys P. h. and Goderis S. (2022) Decoupling of chemical and isotopic fractionation processes during atmospheric entry heating in Antarctic micrometeorites. *Geochim. Cosmochim. Acta*, 221–239.

Lodders K. (1998) A survey of shergottite, nakhlite, and chassigny meteorites whole-rock compositions. *Meteorit. Planet. Sci.* **33**, A183–A190.

Lodders K. (2003) Solar system abundances and condensation temperatures of the elements. *Astrophys. J.* **591**, 1220–1247.

Longhi J. (1992) Experimental petrology and petrogenesis of mare volcanics. *Geochim. Cosmochim Acta* **56**, 2235–2251.

Love S. G. and Brownlee D. E. (1991) Heating and thermal transformation of micrometeoroids entering the Earth's atmosphere. *Icarus* **89**, 26–43.

Lovering J. F. (1975) The Moama eucrite–A pyroxene-plagioclase adcumulate. *Meteoritics* **10**, 101–114.

Lucey P., Korotev R. L., Gillis J. J., Taylor L. A., Lawrence D., Campbell B. A., Elphic R., Feldman B., Hood L. L., Hunten D., Mendillo M., Noble S., Papike J. J., Reedy R. C., Lawson S., Prettyman T., Gasnault O. and Maurice S. (2006) Understanding the Lunar Surface and Space-Moon Interactions. *Rev. Mineral. Geochem.* **60**, 83–219.

Mars Meteorite Compendium. (2003). http://www.curator.jsc.nasa.gov/curator/antmet/mmc/XVLosAngeles03.PDF.

McCarthy T. S., Erlank A. J. and Willis J. P. (1973) On the origin of eucrites and diogenites. *Earth Planet. Sci. Lett.* **18**, 433–442.

McDonough W. F. and Sun S. S. (1995) The composition of the Earth. *Chem. Geol.* **120**, 223–253.

McSween H. Y., Mittlefehldt D. W., Beck A. W., Mayne R. G. and McCoy T. J. (2011) HED meteorites and their relationship to the geology of Vesta and the Dawn Mission. *Space Sci. Rev.* **163**, 141–174.

Metzler K., Bobe K. D., Palme H., Spettel B. and Stöffler D. (1995) Thermal and impact metamorphism on the HED parent asteroid. *Planet. Space Sci.* **43**, 499–525.

Meyer C. (2016). *The Lunar Sample Compendium*. https://curator.jsc.nasa.gov/lunar/lsc/index.cfm.

Mittlefehltdt D. W. (1994) The genesis of diogenites and HED parent body petrogenesis. *Geochim. Cosmochim. Acta* **58**, 1537–1552.

Mittlefehldt D. W. and Lindstrom M. M. (1993) Geochemistry and petrology of a suite of ten Yamato HED meteorites. *Proc. NIPR Symp. Antarct. Meteorites* **6**, 268–292.

Mittlefehldt D. W. and Lindstrom M. M. (2003) Geochemistry of eucrites: Genesis of basaltic eucrites, and Hf and Ta as petrogenetic indicators for altered Antarctic eucrites. *Geochim. Cosmochim. Acta* **67**, 1911–1934.

Mittlefehldt D. W., McCoy T. J., Goodrich C. A. and Kracher A. (1998) Non-chondritic meteorites from asteroidal bodies. In *Planetary Materials* (ed. J. J. Papike). Mineralogical Society of America, Washington DC, pp. 4.01–4.195.

Neal C. R. and Taylor L. A. (1992) Petrogenesis of mare basalts: a record of lunar volcanism. *Geochim. Cosmochim. Acta* **56**, 2177–2211.

Nicklas R. W., Day J. M. D., Vaci Z., Udry A., Liu Y. and Tait K. T. (2021) Uniform oxygen fugacity of shergottite mantle sources and an oxidized martian lithosphere. *Earth Planet. Sci.* **564**, 116876.

Pack A., Höweling A., Hezel D. C., Stefanak M. T., Beck A.-K., Peters S. T. M., Sengupta S., Herwartz D. and Folco L. (2017) Tracing the oxygen isotope composition of the upper Earth's atmosphere using cosmic spherules. *Nat. Commun.* **8**, 15702.

Papike J. J., Hodges F. N., Bence A. E., Cameron M. and Rhodes J. M. (1976) Mare basalts: Crystal chemistry, mineralogy, and petrology. *Rev. Geophys.* **14**, 475–540.

Papike J. J., Ryder G. and Shearer C. K. (1998) Lunar samples. *Rev. Mineral.* **36**, 5.1–5.234.

Papike J. J., Karner J. M. and Shearer C. K. (2003) Determination of planetary basalt heritage: A simple technique using the electron microprobe. *Am. Mineral.* **88**, 469–472.

Papike J. J., Karner J. M., Shearer C. K. and Burger P. V. (2009) Silicate mineralogy of Martian meteorites. *Geochim. Cosmochim. Acta* **73**, 7443–7485.

Patzer A., Hill D. H. and Boynton W. V. (2003) New eucrite Dar al Gani 872: Petrography, chemical composition, and evolution. *Meteorit. Planet. Sci.* **38**, 783–794.

Patzer A., Schluter J., Schultz L., Hill D. H. and Boynton W. V. (2005) The new polymict eucrite Dar al Gani 872: Petrography, chemical composition, noble gas record, and evolution. *Meteorit. Planet. Sci.* **40**, 869–879.

Pun A. and Papike J. J. (1995) Ion microprobe investigation of exsolved pyroxenes in cumulate eucrites: Determination of selected trace-element partition coefficients. *Geochim. Cosmochim. Acta* **59**, 2279–2289.

Righter K. and Drake M. J. (1996) Core formation in Earth's Moon, Mars, and Vesta. *Icarus* **124**, 513–529.

Rochette P., Folco L., Suavet C., van Ginneken M., Gattacceca J., Perchiazzi N., Braucher R. and Harvey R. P. (2008) Micrometeorites from the Transantarctic Mountains. *Proc. Natl. Acad. Sci. U.S.A.* **105**, 18206–18211.

Rojas J., Duprat J., Engrand C., Dartois E., Delauche L., Godard M., Gounelle M., Carillo-Sánchez J. D., Pokorný P. and Plane J. M. C. (2021) The micrometeorite flux at Dome C (Antarctica), monitoring the accretion of extraterrestrial dust on Earth. *Earth Planet. Sci. Lett.* **560**, 116794.

Rubin A. E. and Grossman J. N. (2010) Meteorite and meteoroid: New comprehensive definitions. *Meteorit. Planet. Sci.* **45**, 114–122.

Rudraswami N. G., Genge M. J., Marrocchi Y., Villeneuve J. and Taylor S. (2020) The oxygen isotope compositions of large numbers of small cosmic spherules: Implications for their sources and the isotopic composition of the upper atmosphere. *J. Geophys. Res. Planets*. doi.10.1029/2020JE006414, e2020JE006414.

Ruzicka A., Snyder G. A. and Taylor L. A. (2001) Comparative geochemistry of basalts from the Moon, Earth, HED asteroid, and Mars: Implications for the origin of the Moon. *Geochim. Cosmochim. Acta* **65**, 979–997.

Scott E. R., Greenwood R. C., Franchi I. A. and Sanders I. S. (2009) Oxygen isotope constraints on the origin and parent bodies of eucrites, diogenites, and howardites. *Geochim. Cosmochim. Acta* **73**, 5835–5853.

Soens B., Suttle M. D., Maeda R., Vanhaecke F., Yamaguchi A., van Ginneken M., Debaille V., Claeys P. h. and Goderis S. (2020) Evidence for the presence of chondrule- and CAI-derived material in an isotopically anomalous Antarctic micrometeorite. *Meteorit. Planet. Sci.* **55**, 2703–2726.

Soens B., van Ginneken M., Chernonozkhin S., Slotte N., Debaille V., Vanhaecke F., Terryn H., Claeys P. h. and Goderis S. (2021) Australasian microtektites across the Antarctic continent: evidence from the Sør Rondane Mountain range (East Antarctica). *Geosci. Front.* **12**, 101153.

Stolper E. (1977) Experimental petrology of eucritic meteorites. *Geochim. Cosmochim. Acta* **41**, 587–611.

Stolper E. and McSween H. Y. (1979) Petrology and origin of the shergottite meteorites. *Geochim. Cosmochim. Acta* **43**, 1475–1498.

Suavet C., Alexandre A., Franchi I. A., Gattacceca J., Sonzogni C., Greenwood R. C., Folco L. and Rochette P. (2010) Identification of the parent bodies of micrometeorites with high-precision oxygen isotope ratios. *Earth Planet. Sci. Lett.* **293**, 313–320.

Suavet C., Rochette P., Kars M., Gattacceca J., Folco L. and Harvey R. P. (2011) Statistical properties of the Transantarctic Mountains (TAM) micrometeorite collection. *Polar Sci.* **3**, 100–109.

Suganuma Y., Miura H., Zondervan A. and Okuno J. (2014) East Antarctic deglaciation and the link to global cooling during the Quaternary: evidence from glacial geomorphology and 10Be surface exposure dating of the Sør Rondane Mountains, Dronning Maud Land. *Quat. Sci. Rev.* **97**, 102–120.

Suttle M. D., Dionnet Z., Franchi I. A., Folco L., Greenwood R. C., Gibson J., Rotundi A., King A. and Russell S. S. (2020) Isotopic and textural analysis of giant unmelted micrometeorites – identification of new material from intensely altered ^{16}O-poor water-rich asteroids. *Earth Planet. Sci. Lett.* **546**, 116444.

Suttle M. D., Folco L., Genge M. J., Franchi I. A., Campanale F., Mugnaioli E. and Zhao X. (2021a) The aqueous alteration of GEMS-like amorphous silicate in a chondritic micrometeorite by Antarctic water. *Geochim. Cosmochim. Acta* **293**, 399–421.

Suttle M. D., Hasse T. and Hecht L. (2021b) Evaluating urban micrometeorites as a research resource—A large population collected from a single rooftop. *Meteorit. Planet. Sci.* **56**, 1531–1555.

Takeda H., Mori H. and Bogard D. D. (1994) Mineralogy and ^{39}Ar-^{40}Ar age of an old pristine basalt: Thermal history of the HED parent body. *Earth Planet. Sci. Lett.* **122**, 183–194.

Taylor G. J., Warren P., Ryder G., Delano J., Pieters C. and Lofgren C. (1991) Lunar rocks. In *Lunar Handbook: A User's Guide to the Moon* (eds. G. Heiken, D. Vaniman and B. M. French). Cambridge University Press, Cambridge, pp. 183–284.

Taylor S., Lever J. H. and Harvey R. P. (2000) Numbers, types, and compositions of an unbiased collection of cosmic spherules. *Meteorit. Planet. Sci.* **35**, 651–666.

Taylor S., Alexander C. M. O. 'D., Delaney J., Ma P., Herzog G. F. and Engrand C. (2005) Isotopic fractionation of iron, potassium, and oxygen in stony cosmic spherules: Implications for heating histories and sources. *Geochim. Cosmochim. Acta* **69**, 2647–2662.

Taylor S., Herzog G. F. and Delaney J. S. (2007) Crumbs from the crust of Vesta: Achondritic cosmic spherules from the South Pole water well. *Meteorit. Planet. Sci.* **42**, 223–233.

Taylor S., Jones K. W., Herzog G. F. and Hornig C. E. (2011) Tomography: A window on the role of sulfur in the structure of micrometeorites. *Meteorit. Planet. Sci.* **46**, 1498–1509.

Taylor S., Matrajt G. and Guan Y. (2012) Fine-grained precursors dominate the micrometeorite flux. *Meteorit. Planet. Sci.* **47**, 550–564.

Thiemens M. H., Jackson T., Zipf E. C., Erdman P. W. and van Egmond C. (1995) Carbon dioxide and oxygen isotope anomalies in the mesosphere and stratosphere. *Science* **270**, 969–972.

Treiman A. H. (2005) The nakhlite meteorites: Augite-rich igneous rocks from Mars. *Chem. Erde-Geochem.* **65**, 203–270.

Udry A. and Day J. M. D. (2018) 1.34 billion-year-old magmatism on Mars evaluated from the co-genetic nakhlite and chassignite meteorites. *Geochim. Cosmochim. Acta* **238**, 292–315.

Vaci Z., Day J. M. D., Paquet M., Ziegler K., Yin Q.-Z., Dey S., Miller A., Agee C., Bartischewitz and Pack A. (2021) Olivine-rich achondrites from Vesta and the missing mantle problem. *Nat. Commun.* **12**, 5443.

van Ginneken M., Genge M. J., Folco L. and Harvey R. P. (2016) The weathering of micrometeorites from the Transantarctic Mountains. *Geochim. Cosmochim. Acta* **179**, 1–31.

van Ginneken M., Gattacceca J., Rochette P., Sonzogni C., Alexandre A., Vidal V. and Genge M. J. (2017) The parent body controls on cosmic spherule texture: Evidence from the oxygen isotopic compositions of large micrometeorites. *Geochim. Cosmochim. Acta* **212**, 196–210.

van Ginneken M., Goderis S., Artemieva N., Debaille V., Decrée S., Harvey R. P., Huwig K., Hecht L., Yang S., Kaufmann F. E. D., Soens B., Humayun M., Van Maldeghem F., Genge M. J. and Claeys P. h. (2021) A large meteoritic event of Antarctica ca. 430 ka ago inferred from chondritic spherules from the Sør Rondane Mountains. *Sci. Adv.* **7**, eabc1008.

Van Malderen S. J. M., Van Acker T. and Vanhaecke F. (2020) Sub-micrometer nanosecond LA-ICP-MS imaging at pixel acquisition rates above 250 Hz via a low-dispersion setup. *Anal. Chem.* **92**, 5756–5764.

Wang J., Davis A. M., Clayton R. N., Mayeda T. K. and Hashimoto A. (2001) Chemical and isotopic fractionation during the evaporation of the FeO-MgO-SiO_2-CaO-Al_2O_3-TiO_2-REE melt system. *Geochim. Cosmochim. Acta* **65**, 479–494.

Ward D., Bischoff A., Roszjar J., Berndt J. and Whitehouse M. J. (2017) Trace element inventory of meteoritic Ca-phosphates. *Am. Mineral.* **102**, 1856–1880.

Warren P. H. (2001) Porosities of lunar meteorites: Strength, porosity, and petrologic screening during the meteorite delivery process. *J. Geophys. Res.* **106**, 10101–10111.

Weisberg M. K., McCoy T. J. and Krot A. N. (2006) Systematics and evaluation of meteorite classification. In *Meteorites and the Early Solar System II* (eds. D. S. Lauretta and H. Y. McSween). The University of Arizona Press, Tucson, pp. 19–52.

Wiechert U. H., Halliday A. N., Palme H. and Rumble D. (2004) Oxygen isotope evidence for rapid mixing of the HED meteorite parent body. *Geochim. Cosmochim. Acta* **221**, 373–382.

Wilkening L. L. and Anders E. (1975) Some studies of an unusual eucrite: Ibitira. *Geochim. Cosmochim. Acta* **39**, 1205–1210.

Wood B. J., Smythe D. J. and Harrison T. (2019) The condensation temperatures of the elements: A reappraisal. *Am. Min.* **104**, 844–856.

Yada T., Nakamura T., Noguchi T., Matsumoto N., Kusakabe M., Hiyagon H., Ushikubo T., Sigiura N., Kojima H. and Takaoka N. (2005) Oxygen isotopic and chemical compositions of cosmic spherules collected from the Antarctic ice sheet: implications for their precursor materials. *Geochim. Cosmochim. Acta* **69**, 5789–5804.

Yamaguchi A., Barrat J., Greenwood R., Shirai N., Okamoto C., Setoyanagi T., Ebihara M., Franchi I. and Bohn M. (2009) Crustal partial melting on Vesta: Evidence from highly metamorphosed eucrites. *Geochim. Cosmochim. Acta* **73**, 7162–7182.

Zekollari H., Goderis S., Debaille V., van Ginneken M., Gattacceca J., ASTER Team, Jull T. A. J., Lenaerts J. T. M., Yamaguchi A., Huybrechts P and Claeys P (2019) Unravelling the high-altitude Nansen blue ice field meteorite trap (East Antarctica) and implications for regional palaeo-conditions. *Geochim. Cosmochim. Acta* **248**, 289–310.

Associate editor: James M.D. Day